

**A rapid sedimentary response to the Paleocene-Eocene Thermal
Maximum hydrological change: new data from alluvial units of the
Trempealeau Basin(Spanish Pyrenees)**

Victoriano Pujalte^a, Birger Schmitz^b, Aitor Payros^a

^a Department of Geology, Faculty of Science and Technology, University of the Basque Country UPV/EHU, Bilbao, Spain (Emails: victoriano.pujalte@ehu.eus; a.payros@ehu.eus)

^b Division of Nuclear Physics. Department of Physics, University of Lund, Lund, Sweden (Email: birger.schmitz@nuclear.lu.se).

This is a non-peer reviewed preprint submitted to EarthArXiv.

The original manuscript was submitted to Palaeogeography, Palaeoclimatology Palaeoecology on 11 May 2021 for peer review, yet no reviews were received five months after submission.

Palaeogeography, Palaeoclimatology, Palaeoecology

A rapid sedimentary response to the Paleocene-Eocene Thermal Maximum hydrological change: new data from alluvial units of the Tresp-Graus Basin (Spanish Pyrenees)

--Manuscript Draft--

Manuscript Number:	
Article Type:	Research Paper
Keywords:	Alluvial units; organic carbon isotopes; CIE onset; PETM; Pyrenees
Corresponding Author:	Victoriano Pujalte, Dr University of the Basque Country: Universidad del Pais Vasco Leioa, Bizkaia SPAIN
First Author:	Victoriano Pujalte, Emeritus Professor
Order of Authors:	Victoriano Pujalte, Emeritus Professor Birger Schmitz, Professor Aitor Payros, Lecturer
Manuscript Region of Origin:	Europe
Abstract:	<p>Abstract</p> <p>A massive emission of light carbon about 56 Ma ago, recorded in marine and terrestrial sediments by a negative carbon isotope excursion (CIE), caused a short-lived (~170 kyr) global warming event known as the Paleocene–Eocene Thermal Maximum (PETM). The core of this event is represented in the south Pyrenean Tresp-Graus Basin by two successive alluvial units, the Claret Conglomerate (CC) and the Yellowish Soils, which represent laterally juxtaposed depositional environments. It is generally agreed that these units record a dramatic increase in seasonal rain and an increased intra-annual humidity gradient during the PETM, but the timing of the sedimentary response to the hydrological change is a matter of debate. Some authors maintain that the CC was developed during the early, most intense phase of the carbon emission, others that its formation lagged by 16.5 ± 7.5 kyr behind the onset of the PETM. The latter claim was mainly based on the assumption that in two sections of this basin, Claret and Tendrui, the onset of the CIE occurs 3 and 8 m below the base of the CC, respectively. Here we show that in the zone between these two sections the CC is missing and the Yellowish Soil unit rests directly and conformably on the underlying deposits. New $\delta^{13}\text{C}_{\text{org}}$ data from this zone provide sound evidence that the onset of the CIE is situated just ~1 m below the Yellowish Soils. The CC erosional base cuts down deeper than this figure, rendering it highly unlikely the preservation of the CIE onset below it. A tentative estimate based on sedimentation rates indicates that ~3.8 kyr, or less, may have elapsed from the onset of the CIE to the arrival of PETM alluvium into the Claret-Tendrui study area, about a third of the lowest estimate of previous authors. Since the study area was situated about 15 km from the source area, our new estimate supports a rapid response of the sedimentary system to the hydrological change at the onset of the PETM.</p>

Highlights – Pujalte et al

The PETM hydrological change is recorded in the Pyrenees by two alluvial units

Between the PETM onset and the alluvial accumulation a lag of ~3.8 kyr is estimated

The new data entail a rapid sedimentary response to the PETM hydrological change

1 **A rapid sedimentary response to the Paleocene-Eocene Thermal Maximum**
2 **hydrological change: new data from alluvial units of the Tresp-Graus Basin**
3 **(Spanish Pyrenees)**

4 Victoriano Pujalte^a *, Birger Schmitz^b, Aitor Payros^a

5 ^a *Department of Geology, Faculty of Science and Technology, University of the Basque*
6 *Country UPV/EHU, Bilbao, Spain*

7 ^b *Division of Nuclear Physics. Department of Physics, University of Lund, Lund, Sweden*

8 * Corresponding author. *E-mail address:* victoriano.pujalte@ehu.eus.

9 **Abstract**

10 A massive emission of light carbon about 56 Ma ago, recorded in marine and terrestrial
11 sediments by a negative carbon isotope excursion (CIE), caused a short-lived (~170 kyr)
12 global warming event known as the Paleocene–Eocene Thermal Maximum (PETM).
13 The core of this event is represented in the south Pyrenean Tresp-Graus Basin by two
14 successive alluvial units, the Claret Conglomerate (CC) and the Yellowish Soils, which
15 represent laterally juxtaposed depositional environments. It is generally agreed that
16 these units record a dramatic increase in seasonal rain and an increased intra-annual
17 humidity gradient during the PETM, but the timing of the sedimentary response to the
18 hydrological change is a matter of debate. Some authors maintain that the CC was
19 developed during the early, most intense phase of the carbon emission, others that its
20 formation lagged by 16.5 ± 7.5 kyr behind the onset of the PETM. The latter claim was
21 mainly based on the assumption that in two sections of this basin, Claret and Tendrui,
22 the onset of the CIE occurs 3 and 8 m below the base of the CC, respectively. Here we
23 show that in the zone between these two sections the CC is missing and the Yellowish
24 Soil unit rests directly and conformably on the underlying deposits. New $\delta^{13}\text{C}_{\text{org}}$ data
25 from this zone provide sound evidence that the onset of the CIE is situated just ~1 m
26 below the Yellowish Soils. The CC erosional base cuts down deeper than this figure,
27 rendering it highly unlikely the preservation of the CIE onset below it. A tentative

28 estimate based on sedimentation rates indicates that ~3.8 kyr, or less, may have elapsed
29 from the onset of the CIE to the arrival of PETM alluvium into the Claret-Tendrui study
30 area, about a third of the lowest estimate of previous authors. Since the study area was
31 situated about 15 km from the source area, our new estimate supports a rapid response
32 of the sedimentary system to the hydrological change at the onset of the PETM.

33 Key words: Alluvial units; organic carbon isotopes; CIE onset; PETM; Pyrenees

34 **1. Introduction**

35 The long-term environmental impact of the ongoing global warming is a matter of great
36 concern and debate. One of its predicted effects is an alteration of the hydrological
37 cycle, because a warmer atmosphere can hold more moisture (Held and Soden, 2006).
38 However, the timing of the sedimentary response to such environmental changes
39 remains uncertain. One way to predict these effects is modelling (Deser et al., 2020).
40 For example, the modelling of river behaviour by Simpson and Castelltort (2012, p.1134)
41 showed that variations in water discharge likely transmit, and can even amplify,
42 sedimentary signals to downstream archives. Examples from modern alluvial systems
43 also indicate that the sedimentary reaction to large rainfall events can be nearly
44 instantaneous. For instance, an exceptional rainstorm (locally > 600 l/m²) in the semi-
45 arid southeast of the Iberian Peninsula caused a catastrophic flood on October 18, 1973
46 (Capel Molina, 1974), after which a small fan delta in the coastal village of La Rábita
47 experienced a seaward progradation of up to 270 m (Fig. 1).

48 An alternative way to learn about the sedimentary response to global warming and
49 concomitant changes of the hydrological cycle is the study of past analogues, such as
50 the Paleocene–Eocene Thermal Maximum (PETM), a short-lived (~170 kyr) global
51 warming event that increased Earth's temperature by ~5-8 °C about 56 Ma ago. It was

52 caused by a massive injection of light carbon into the ocean-atmosphere reservoirs,
53 which was recorded in marine and terrestrial deposits by a prominent negative carbon
54 isotope excursion (CIE) (Koch et al., 1992; Sluijs et al. 2007; Zachos et al. 2008;
55 McInerney and Wing 2011). Hydrological changes induced by the PETM have been
56 reported in numerous studies. For instance, this event caused abrupt changes in alluvial
57 architecture in the Piceance Creek Basin, Colorado, (Foreman et al., 2012; Foreman,
58 2014) and the Uinta Basin, Utah (Plink-Björklund et al., 2014), as well as an alteration
59 of the stacking pattern and type of paleosols in the terrestrial Big Horn Basin, Wyoming
60 (Kraus et al., 2013, 2015). Increased influx of terrestrial clays attributed to intensified
61 rainfall and runoff have also been reported from widely separated continental margins
62 (Gibson et al., 2000; Schmitz et al., 2001; John et al., 2008; Handley et al., 2012;
63 Slotnick et al., 2012), while a massive input of both fine- and coarse-grained
64 siliciclastics temporarily halted a long-lasting carbonate deposition in shallow marine
65 areas of the Pyrenees (Pujalte et al., 2016; Pujalte and Schmitz, 2019) and the Xigaze
66 forearc basin of the Tibet (Jiang et al., 2021).

67 The Claret Conglomerate (CC) of the Tresp-Graus Basin (southern Pyrenees), the
68 focus of this study, is another prominent and amply referenced case (Schmitz and
69 Pujalte, 2003, 2007; Armitage, et al., 2011, 2013; Foreman et al., 2012; Minelli et al.,
70 2013; Foreman, 2014; Pancost, 2017; Colombero et al., 2017; Allen, 2017; Carmichael
71 et al., 2017, 2018). However, the time relationship between the PETM hydrological
72 change and the sedimentary response recorded by the CC has created some discussion.
73 Schmitz and Pujalte (2007), for instance, suggested that the CC was accumulated during
74 the first 10 kyr, or less, of the PETM, which implies a rapid sedimentary response.
75 Instead, Domingo et al. (2009), Manners et al. (2013) and Duller et al. (2019)
76 (henceforward referred to collectively as DMD 09-19), mainly based on the study of

77 $\delta^{13}\text{C}_{\text{org}}$ of two sections (Claret and Tendrui, here named Claret road and T_{DMD}),
78 concluded that the onset of the thermal event predated the CC by 16.5 ± 7.5 kyr and
79 postulated a delayed response of the sedimentary system to the PETM hydrological
80 change.

81 A first purpose of this paper is to address this discrepancy. To this end, a detailed field
82 study has been carried out in an area situated to the west of Tresp (study area in
83 Supplementary Fig. 1A). Eight reference Paleocene-Eocene boundary sections were
84 studied and sampled, including the controversial Claret and T_{DMD} sections, and a
85 detailed field mapping of their surroundings was undertaken with the aim of gaining a
86 wider perspective. As a result, the internal architecture of the CC in this area has been
87 documented for the first time, shedding new light on the development of the unit. In
88 addition, an attempt is made to estimate the rate of the sedimentary change induced by
89 the PETM hydrological change, as recorded by the arrival of PETM alluvial clastics to
90 the study area.

91 **2. Geological setting, stratigraphy and prior information**

92 In early Paleogene times the Tresp-Graus Basin was situated in the southeastern part of
93 the Pyrenean marine gulf, an E-W elongated embayment opening westwards into the
94 Bay of Biscay at $\sim 35^\circ\text{N}$ palaeolatitude (Fig. 2A; Baceta et al., 2011; Pujalte et al.,
95 2016). The eastern part of the basin was mostly infilled with terrestrial deposits (Fig.
96 2B), informally named “Garumnian” (Rosell et al., 2001) and formally Tresp Group
97 (Cuevas, 1992; Pujalte and Schmitz, 2005; Pujalte et al., 2014). This Group is
98 sandwiched between shallow marine deposits, the Maastrichtian Aren Sandstone
99 Formation below and the informal “Alveolina limestone” unit above (Ilerdian = lower

100 Ypresian), and interfingers to the west with lacustrine and shallow marine carbonates
101 (Pujalte et al., 2014).

102 In the Tremp-Graus Basin the PETM interval was first identified by Schmitz and Pujalte
103 (2003) in the Esplugafreda section, mainly based on analyses of $\delta^{13}\text{C}$ of soil carbonate
104 nodules (Supplementary Figs. 2A, B). Ten years later Manners et al (2013) studied the
105 isotopic composition of dispersed organic carbon of bulk samples ($\delta^{13}\text{C}_{\text{org}}$) across the
106 Paleocene-Eocene boundary (P-E) interval of this section, placing the PETM in the
107 same position (Supplementary Fig. 2C).

108 In the present study area, situated about 10 km to the south of Esplugafreda and just
109 west of the city of Tremp (Fig. 2B, Supplementary Fig. 1), the P-E boundary interval
110 comprises four of the five lithostratigraphic units recognized at Esplugafreda (Fig. 2C),
111 their characteristics being summarized below from older to younger.

112 The Esplugafreda Formation (Thanetian, ~350 m thick at Claret) is mostly made up of
113 overbank red and variegated silty mudstones with irregular intercalations of channelized
114 calcarenites and calcareous conglomerates. The red mudstones include soil carbonate
115 nodules, *Microcodium* (submillimeter-sized monocrystalline prisms of calcite originated
116 on roots of terrestrial plants) and a whole range of gypsum facies, from rosettes and
117 root-like molds to massive alabastrine accumulations up to 4 m thick, interpreted as
118 deposits of ephemeral saline lakes (García-Veigas, 1988), all of which provide evidence
119 of semiarid to arid conditions.

120 The incised valley fill occurs within an erosional depression ca. 1.5 km wide and up to
121 30 m deep excavated on the Esplugafreda Formation during a lowstand period predating
122 the PETM (Fig. 2D; Pujalte et al., 2014). The lithological composition of this infill is
123 markedly different to that of the Esplugafreda Formation. It comprises coarse-grained

124 imbricated conglomerates in its lower part that record westward flowing currents (Figs.
125 3A, B). The bulk of the unit, however, consists of alternating light gray calcarenites and
126 marlstones devoid of carbonate nodules but rich in coalified remains, including
127 occasional amber fragments, and even a small tree trunk buried in living position (Figs.
128 3C, D). The grey colours and abundant preservation of organic material are indicative of
129 reducing conditions, probably in an aquatic/riparian setting. A minor but significant part
130 of this unit consists of red mudstones with scattered soil carbonate nodules indicative of
131 well-oxygenated conditions (Fig. 4A), their location attesting to the final infilling of the
132 incised valley (Fig. 2D). Interestingly, the uppermost 30 cm of the red mudstones are
133 intensely altered (Fig. 4B). The altered zone contains abundant carbonate nodules that
134 can be easily crushed and can hence be considered (sub)recent, an indication that the
135 alteration was produced by hard waters percolating through the overlying CC.
136 Alteration of sediments situated just below the CC has also been observed in other
137 sections (e.g. Supplementary Fig. 3A).

138 The CC is an extensive sheet-like unit up to 4 m thick, of clast-supported calcareous
139 conglomerates, pebbly calcarenites and minor mudstones, further described below. The
140 Yellowish soil unit is up to 20 m thick in the study area and mainly consists of fine-
141 grained mudstones of a light yellow colour in weathered exposures, with intercalated
142 calcarenite channels 1-5 m thick but modest lateral extent (5–20 m). The mudstones
143 contain abundant small-sized (≤ 1 cm) soil carbonate nodules evenly distributed
144 throughout the unit, but neither *Microcodium* nor gypsum have been observed. In
145 proximal areas of the basin (e.g., Esplugafreda, Supplementary Fig. 1A) the Yellowish
146 Soils always overlie the CC. However, according to the Walther's Law of Facies, both
147 units represent frontally juxtaposed depositional environments, which imply that the CC
148 must grade distally into the Yellowish Soils.

149 The uppermost gypsum-rich unit is usually represented by red mudstones crisscrossed
150 by gypsum veins and rosettes and locally by a 4 m thick package of massive alabastrine
151 gypsum. In some section this massive gypsum package is overlain by fresh-water
152 limestones which yielded post-PETM $\delta^{13}\text{C}_{\text{carb}}$ values (Schmitz and Pujalte, 2003.
153 Supplementary Fig. 3B).

154 Previous isotope records from soil carbonate nodules ($\delta^{13}\text{C}_{\text{carb}}$; Schmitz and Pujalte,
155 2003, 2007; Pujalte et al., 2014; Minelli et al., 2013) and from bulk dispersed organic
156 matter in the Esplugafreda section ($\delta^{13}\text{C}_{\text{org}}$; Manners et al., 2013, Supplementary Fig.
157 2C) indicate that the Esplugafreda Formation and the incised valley fill deposits predate
158 the PETM, the CC and the Yellowish Soils encompass the core of the thermal event,
159 while the recovery to pre-event background conditions is recorded in the gypsum-rich
160 unit. However, the onset of the CIE in the study area is controversial. Schmitz and
161 Pujalte (2003), Pujalte and Schmitz (2005) and Pujalte et al. (2009) placed it at the base
162 of the CC, whereas DMD (09-19) maintain that it occurs below the CC, at about -3 m in
163 the Claret section (here called Claret road; Fig. 2C) and -8 m in the T_{DMD} section.

164 **3. Material and methods**

165 This study is mainly based on field observations, aided with satellite images of Google
166 Earth and the Institut Cartogràfic i Geològic de Catalunya. The P-E boundary interval
167 succession of the study area was re-mapped and the best outcrops photographed with a
168 digital camera to facilitate the analysis of their facies and depositional architecture.
169 Palaeocurrents were obtained from cross-bedding and the orientation of large scale
170 dunes.

171 Previously published $\delta^{13}\text{C}_{\text{carb}}$ isotopic data from Schmitz and Pujalte (2003), Pujalte et
172 al. (2009) (Supplementary Fig. 3B) and $\delta^{13}\text{C}_{\text{org}}$ isotopic data from DMD (09-19) were
173 reassessed. In addition, nine sections were studied in detail, in eight of which 100 new
174 samples were collected to analyze the isotopic composition of dispersed organic carbon.
175 To this end, the hardest pieces of the samples (i.e. the best preserved) were cleaned with
176 distilled water to eliminate surface dust, dried at 30° in an oven for 24 hours and finely
177 ground on an agate mortar. The resulting powdered samples were analyzed for $\delta^{13}\text{C}$ of
178 bulk dispersed organic matter at the Servicios de Apoyo á Investigación (SAI) of the
179 University of A Coruña, Spain. Powdered samples were weighed (400 μg) into 12 mL
180 exetainers, sealed, and then flushed with helium to displace and replace the air
181 contained above the samples. After the flushing process was complete, about 100 μL of
182 ortho-phosphoric acid were added to each sample. The samples were kept at 26°C and
183 left to react with the acid for 24 h. The resulting headspace CO_2 was passed through a
184 Poraplot Q fused silica capillary column (25 m, 0.32 mm, Varian) maintained at 70°C,
185 and finally through a capillary was introduced into the ionization chamber of a mass
186 spectrometer. The carbon isotope ratio of CO_2 gas extracted from solid samples was
187 measured using a ThermoFinnigan MAT253 isotope ratio mass spectrometer interfaced
188 with a ThermoFinnigan Gas Bench II device and a GC-PAL autosampler (CTC
189 Analytics). The system was calibrated with NBS19, NBS18 and LSVEC standards,
190 supplied by IAEA, Vienna, Austria. The results are reported with the conventional delta
191 notation with respect to VPDB (Vienna Pee Dee Belemnite).

192 **4. Results**

193 The CC is discontinuous in the study area, probably due to its relatively distal location
194 (~15 km to the south of the source area, Supplementary Fig. 1). When the CC is absent,

195 the Esplugafreda Formation is directly overlain by the Yellowish Soils (Figs. 2C, D).
196 Thus, the P-E boundary interval successions present some significant differences in the
197 Claret and Tendrui sectors, as well as in the intervening St Adria valley. These three
198 zones are described separately below.

199 *4.1. The P-E boundary interval in the Claret sector*

200 The CC stretches for about 1.5 km in a N-S transect of the Claret sector, from the Palau
201 creek in the south to the Ricos creek in the north, almost everywhere overlying the
202 incised valley deposits (Figs. 2C, D). Due to its weathering resistant nature, the CC has
203 created a cuesta landform, the top surface of which is widely exposed on the west-
204 dipping gentle slope. This surface is generally sharp and nearly flat and is crisscrossed
205 by a conspicuous conjugate set of joints, clearly noticeable in satellite images
206 (Supplementary Figs. 4A, B). In turn, the CC has created a small cliff in the cuesta steep
207 slope (Supplementary Fig. 4D).

208 Four sections have been studied in this sector, three of which were sampled (Fig. 2D).
209 The Claret north, Claret hamlet and Palau sections are illustrated in Figs. 5 and 6 and
210 briefly described below. The fourth one, the Claret road section, is dealt with in more
211 detail in the next point, both to clarify the position of the base of the CIE and because it
212 provides important clues about the internal architecture and development of the CC.

213 *4.1.1. The Claret north, Claret hamlet and Palau sections*

214 In the Claret north section, which is oriented nearly perpendicular to palaeocurrents
215 (Fig. 5A), the CC is about 4 m thick and it is made up of stacked tabular packages of
216 clast-supported conglomerates and lesser amounts of pebbly sandstones delimited by
217 erosional surfaces (Fig. 5B). The lower boundary of the CC is sharp and slightly
218 erosional, cutting ~ 60 cm into well exposed grey calcarenites and marlstones of the

219 incised valley fill. The Palau creek section offers a NE-SW oriented vertical exposure,
220 near parallel to palaeocurrents, in which large-scale unidirectional cross-bedding can be
221 observed (Fig. 5C). Taken together, these two sections permit a 3D reconstruction of the
222 internal architecture of the unit, providing a first indication of its south-westwards
223 progradation.

224 The incised valley fill deposits situated just below the CC were analyzed for organic
225 carbon isotopes in the Claret north and Claret hamlet sections (Fig. 6). The former
226 exposes ~2 m of grey calcarenites and marls, from which 15 samples were collected at
227 close-spaced intervals. The lower 10 samples provided a vertical stable trend, with
228 $\delta^{13}\text{C}_{\text{org}}$ values ranging between -22 and -23.6‰ (in black in Fig. 6A). Four out of the
229 upper five samples, collected in the 20 cm interval situated just below the CC, also
230 yielded low values (-22.7 to -24.2‰), the remaining one being somewhat more negative
231 (-25.2‰; red in Fig. 6A).

232 In the Claret hamlet section the CC is underlain by about 5 m of red calcareous
233 mudstones with scattered soil carbonate nodules. $\delta^{13}\text{C}_{\text{org}}$ values from four bulk samples
234 of the red mudstones gave values between -24.4 and -23.9‰ (Fig. 6B). In this same
235 section Pujalte et al. (2009) reported the $\delta^{13}\text{C}_{\text{carb}}$ values of three nodules samples,
236 respectively -7.3, -7.6 and -7.7‰ (Supplementary Fig. 3B).

237 *4.2.2. The Claret road section*

238 The P-E boundary interval of the Claret road section is exposed in the trench of the road
239 C-1311 from Trepmp to the Montllobat Pass, near km 22. Due to its easy access it is the
240 most studied and referenced section of the Claret sector (Pujalte and Schmitz, 2005;
241 Pujalte et al., 2009; Domingo et al., 2009; Minelli et al., 2013; Manners et al., 2013;
242 Pujalte and Schmitz, 2014; Payros et al., 2016; Duller et al. 2019). However, a major

243 problem with this section is that the boundary between the incised valley deposits and
244 the CC is not exposed, as it is covered up by a dense thicket of bushes and trees (Fig.
245 7A, Supplementary Fig. 5A). To overcome the problem, the scattered outcrops of the
246 CC within the thicket were mapped in this study and connected with the road exposure.
247 The uppermost incised valley deposit exposed in the road is a ~1 m thick calcarenite
248 bed (“reference calcarenite”), the CC base being situated about 2 m above it (Figs. 7B,
249 C). Between the reference calcarenite and the CC base vegetation and a thick recent soil
250 preclude digging out fresh samples.

251 The CC is well outcropped in the road trench to the west of the thicket, but the
252 underlying incised valley deposits are not exposed therein (Fig. 8). The CC is mainly
253 composed of calcareous conglomerates and pebbly calcarenites, but it also contains
254 sizable intercalations of marly clays. Cross-stratifications in some of the conglomeratic
255 beds consistently indicate west-directed palaeocurrents (Fig. 8), which demonstrates
256 that the road trench provides a near dip oriented view of the CC. A large scale low-
257 angle cross-stratification of the CC coarse beds is also evident, which denotes a
258 westward progradation of the unit (Fig. 8A).

259 Pinpointing the top of the CC in the road trench itself is difficult because the unit is
260 there directly overlain by one of the younger calcarenite channels intercalated in the
261 Yellowish Soils. However, the near flat upper surface of the CC is widely exposed just
262 north of the road, being readily recognizable by its tell-tale conjugate set of joints (Fig.
263 7A, Supplementary Figs. 5B, C). Tracing this surface to the road trench demonstrates
264 that the alleged CC base in DMD (09-19) is actually situated only about 1 m below the
265 top of the unit (Fig. 8A, Supplementary 5D). This circumstance inescapably demands
266 that the samples collected by DMD (09-19) ~3 m below their CC base, which provided

267 PETM values, must have been taken from marly clays intercalated within the CC, as
268 indicated by Pujalte and Schmitz (2014).

269 In this study six samples were collected for organic carbon isotope analysis, three from
270 the incised valley deposits and three from the marly clays of the CC (Figs. 7C, 8A).
271 Those of the incised valley fill provide $\delta^{13}\text{C}_{\text{org}}$ values between -23.1 and -23.6‰,
272 whereas those of the CC range between -25.3 and -26.1‰, averaging out at -25.6‰.

273 *4.2. The P-E boundary interval in St Adria valley*

274 The St Adria creek has excavated a narrow valley that in its lower reach is about 80 m
275 deep and exposes the entire P-E interval in both of its steep margins (Fig. 2C). The CC
276 is discontinuous and only occurs on the southern one (Fig. 2C). When the CC is absent
277 the uppermost part of the Esplugafreda Formation consists of red silty marls with
278 abundant CaCO_3 soil nodules capped by a 30–50 cm thick interval of clays with a
279 conspicuous purple colour (Fig. 9A). This “purple cap”, which is devoid of carbonate
280 nodules but contains numerous small diameter (≤ 1 mm) ferruginous nodules (Fig 9B),
281 was found in every accessible outcrop of the St Adria valley in which the CC is absent,
282 a proof that it is not a localized feature. The Yellowish Soils overlie directly and
283 conformably this purple cap.

284 Two separate CC packages are observable on the southern margin of the valley, both of
285 them almost entirely encased within the Esplugafreda Formation (Figs. 10A, B). The
286 one situated to the WNW is about 150 m wide and 2 m thick (Fig. 10B). In the zone
287 between both CC packages a section, coded Ad-S, was sampled at close-spaced
288 intervals across the Esplugafreda/Yellowish Soils transition (Figs. 10C, D). The five
289 samples situated between -230 and -140 cm below the boundary gave a narrow range of
290 $\delta^{13}\text{C}_{\text{org}}$ values (from -22.3 to -22.7‰). However, between -1 m and the

291 Esplugafreda/Yellowish Soils boundary, $\delta^{13}\text{C}_{\text{org}}$ values became gradually more
292 negative, first slowly and then rapidly, peaking at a minimum of -28.5‰ in the purple
293 cap (Fig. 10C). Values of five samples analyzed from the overlying Yellowish Soils
294 remain quite negative, ranging between -24.9 and -26.6‰.

295 The Esplugafreda/Yellowish soil boundary is also well exposed to the west of the
296 WNW termination of the CC, except where a calcarenite channel intercalated in the
297 Yellowish locally impinges on the Esplugafreda Formation (Figs 10E). Below both the
298 CC and the calcarenite channel, the purple cap has been eroded away.

299 On the northern margin of the St Adria valley the Yellowish Soils unit generally rests
300 directly on the Esplugafreda Formation, as the CC is there absent. Two sections from
301 this margin were analyzed, coded Ad-N₁ and Ad-N₂, respectively (Fig. 11A). A reduced
302 purple cap is discernible in the former (Figs. 11B). In the upper 2.75 m of the
303 Esplugafreda Formation, which have a similar composition to that in the AD-S section,
304 including abundant carbonate nodules (Fig. 11C), seventeen mudstone samples were
305 collected for organic carbon isotope analysis. Values of the lower thirteen of these
306 samples vary between -22.3 and -23.4 ‰, averaging out at -22.7 ‰, but in the
307 uppermost 0.5 m of the Esplugafreda Formation values gradually decrease, peaking at -
308 25.8 ‰ in the purple cap (Fig. 11B).

309 The Ad-N₂ section encompasses the uppermost 30 m of the Esplugafreda Formation,
310 which are composed of alternating grey gypsiferous marls and red and variegated
311 mudstones rich in carbonate nodules. The top of the Esplugafreda Formation is abruptly
312 truncated by a 2 m thick calcarenite channel, in turn overlain by the Yellowish Soils
313 (Figs 11A, D). The $\delta^{13}\text{C}_{\text{org}}$ values throughout the Esplugafreda Formation are quite
314 stable, varying between -23 and -24‰ and averaging out at 23.5‰. A more negative

315 value (-27‰) is recorded in the calcarenite channel, the negative values (-26‰)
316 persisting within the overlying Yellowish Soils (Fig. 11D).
317 Schmitz and Pujalte (2003) sampled at low resolution another section of the St Adria
318 northern margin situated about 200 m to the WNW of the Ad-N₁ section (S&P 2003 in
319 Fig. 2D). The exposed part of the Esplugafreda Formation successively comprised grey
320 marls with gypsum, red mudstones with carbonate nodules and the purple cap. Only one
321 nodule sample was collected from the red marls, which produced a $\delta^{13}\text{C}_{\text{carb}}$ value of –
322 8.6‰, whereas values of seven nodule samples from the Yellowish Soils varied
323 between -12 to -14‰ (Supplementary Fig. 3B).

324 *4.3. The P-E boundary interval in the Tendrui sector*

325 The CC is about 1–3 m thick and stretches for about 200 m in S-N direction in the
326 Tendrui sector, where it rests on the Esplugafreda Formation (Fig 2C). It is overgrown
327 with trees that prevent a proper assessment of its internal geometry. Neither can the
328 nature of the sediments overlying the unit be established, as a farmland exists just above
329 it (Fig. 11A).

330 Field observations indicate that in the Tendrui sector the CC is also encased within the
331 Esplugafreda Formation. Visually this can to be observed in the southern termination of
332 the CC, but the encasement depth cannot be verified because of the farmland (Fig.
333 11A). In the northern part of the CC outcrop, however, it has been confirmed that the
334 top of the CC is situated about 1 m below the base of the Esplugafreda
335 Formation/Yellowish soil boundary.

336 Two sections located close to each other have been studied in the northern part of the
337 Tendrui sector, the T_{DMD} described by DMD (09-19) and one situated in the trench of a

338 dirt tract about 40 m to the north, coded T_{dt} (Fig. 12A). The part of the T_{DMD} section
339 revisited in this study is situated in a small vegetated ravine (Figs. 12A, B; cf., small
340 photo in fig. 3 of Domingo et al., 2009). It comprises a 20 m thick segment of the
341 Esplugafreda Formation situated immediately below the CC, the lowermost part of
342 which is formed by red calcareous mudstones with carbonate nodules, the remainder by
343 brownish silty marls devoid of nodules and gypsum (Fig. 12B, C). DMD (09-19)
344 analyzed about 20 samples from this interval, their values being plotted in Fig. 12C
345 (small diamonds, yellow in the online version). Values of five samples collected for this
346 study (large diamonds, red in the online version, Fig. 12C) are roughly similar to those
347 of DMD (09-19). While collecting them it was noticed that the marls become
348 increasingly softer and discoloured up to the CC.

349 The nearby T_{dt} section (Fig. 12A) comprised the 8 m thick interval of the Esplugafreda
350 Formation situated just below the CC. Today this section is vegetated only in its upper
351 part, but the excavation of the dirt track trench unearthed numerous subvertical large
352 roots coming down throughout the section from the trees above (Fig. 12D). The section
353 is largely covered by loose clays, but well-indurated grey-brownish silty marls are
354 exposed along several small vertical rills coming down through most of the section,
355 from which six samples were collected (Fig. 12D). The lower five samples were well
356 indurated and gave $\delta^{13}\text{C}_{\text{org}}$ values ranging from -24.1‰ to -24.8‰, averaging out at
357 24.4‰ (Fig. 12E). The uppermost marl sample, collected in the upper vegetated part of
358 the section, was soft and contained numerous traces of recent roots, yielding a $\delta^{13}\text{C}_{\text{org}}$
359 value of -25.2‰.

360 **5. Discussion**

361 *5.1. Architecture of the Claret Conglomerate*

362 The predominant coarse-grained components of the CC must have been transported by
363 powerful currents, a fact that explains both the erosional base of the unit
364 (Supplementary Fig. 3A) and its encasement in the Esplugafreda Formation (Figs. 2D,
365 10A, B). Palaeocurrents from cross-bedding and large-scale dunes demonstrate that
366 these currents preferentially flowed to the WSW (Fig. 5A), similar to those indicated by
367 the clast imbrications in the basal conglomerates of the incised valley. This
368 circumstance and the areal concurrence of the incised valley and the CC outcrops
369 suggest that the latter unit was mainly accumulated in a residual depression of the
370 former, which probably explains the lens-like CC shape in the Claret sector (Fig. 2D).
371 Instead, where the CC overlies the Esplugafreda Formation it exhibits a near tabular
372 shape (e.g., Fig. 10B).

373 The most significant internal architectural features of the CC are observed in the Claret
374 road section. The slope of the low-angle inclined conglomeratic strata coincides with
375 the direction indicated by the palaeocurrents (Fig. 8A). These strata, therefore, must
376 record a forward progradation of the CC during episodes of strong currents. Conversely,
377 silty clays intercalated between the conglomerate strata must have been accumulated in
378 quieter conditions, from which it seems logical to conclude that the progradation of the
379 CC was intermittent, with alternating periods of activity and stillness.

380 *5.2. Onset of the CIE in the study area*

381 Interpretation of $\delta^{13}\text{C}_{\text{org}}$ results obtained from bulk rocks must be treated with caution,
382 because they may reflect variations in the proportion of autochthonous and
383 allochthonous organic components and/or different degrees of diagenetic degradation.
384 In marine deposits the reliability of $\delta^{13}\text{C}_{\text{org}}$ curves can be validated (or disproved)
385 through a comparison with other indicators, mainly biostratigraphic data (e.g. Storme et

386 al., 2012). Such a procedure, however, is seldom applicable in terrestrial deposits,
387 which are either barren or poorly fossiliferous, as it is the case of the successions here
388 considered. One possible way to circumvent these problems is to analyze high-
389 molecular weight n-alkanes (C25 to C33), which have a higher resistance to isotopic
390 exchange (Baczynski et al., 2016). However, even this procedure does not always
391 guarantee accurate results (e.g., Baczynski et al., 2019).

392 Consequently, the following four criteria have been used in this study to evaluate the
393 significance of the $\delta^{13}\text{C}_{\text{org}}$ profiles: (1) $\delta^{13}\text{C}_{\text{org}}$ values from pre-PETM deposits vary
394 between -22 and -25‰ and those from PETM deposits between -25 and -27‰, a
395 criterion previously used, for instance, by Yans et al. (2014) and Maufrangeas et al.
396 (2020) in sections of the northern Pyrenees; (2) the onset of the CIE entails a *sustained*
397 shift of -2 to -3‰; (3) comparisons between different $\delta^{13}\text{C}_{\text{org}}$ isotopic profiles of the
398 area, as well as with $\delta^{13}\text{C}_{\text{carb}}$ profiles when available; (4) last, but not least, field
399 relationships of the studied sections were taken into account.

400 The isotopic profiles obtained independently by Schmitz and Pujalte (2003) and
401 Manners et al. (2013) in the Esplugafreda section exemplify the application of these
402 criteria (Supplementary Fig. 2). Thus, $\delta^{13}\text{C}_{\text{org}}$ values ranging from -21.5 to -23.5‰ were
403 considered pre-PETM and those between -24.9 and -26.5‰ ascribed to the PETM by
404 Manners et al. (2013). However, a ~1.5‰ shift found by the Manners et al. (2013)
405 between the Esplugafreda Formation and the incised valley fill deposits was considered
406 of no significance. Likewise, a ~2‰ shift in $\delta^{13}\text{C}_{\text{carb}}$ profile found by Schmitz and
407 Pujalte (2003) ~70 m below the CC was dismissed on the same basis. However, both
408 studies constrained the PETM to the same interval of the Esplugafreda section, mutually
409 reinforcing the validity of independent criteria.

410 An application of the aforementioned criteria in the study area reveals that the isotopic
411 shift most likely associated to the onset of the CIE is the one recorded in the uppermost
412 part of the Esplugafreda section in the Ad-S and Ad-N₁ sections of the St Adria valley
413 (Figs. 10B, 11B). This shift, which is based on high-resolution $\delta^{13}\text{C}_{\text{org}}$ profiles, is both
414 gradual and persistent, its shape and magnitude (2-4‰) being similar to the one found
415 in terrestrial sections elsewhere (e.g., Baczynski et al., 2013). Finally, this shift is
416 situated in the position predicted in the low resolution $\delta^{13}\text{C}_{\text{carb}}$ profile reported by the
417 Schmitz and Pujalte (2003) in another section of the St Adria valley (Fig. 2D,
418 Supplementary Fig. 3B).

419 In the other section studied in this valley (Ad-N₂; Figs. 11D) $\delta^{13}\text{C}_{\text{org}}$ values from the
420 Esplugafreda Formation provide pre-PETM values (-23 to -24‰), and those of the
421 Yellowish Soils PETM values (-26.1‰ on average). However, the gradual shift which
422 marks the CIE onset in the Ad-S and Ad-N₁ sections is not recorded, a fact readily
423 attributable to the truncation of the top of the Esplugafreda section by a calcarenite
424 channel.

425 Field evidence indicates that the top of the CC in the Tendrui sector is situated ~1m
426 below the base of the Yellowish Soils in the adjacent St. Adria sector (Fig. 11A).
427 Consequently, the CIE onset proposed by DMD (09-19) would be located about 11 m
428 lower than its actual position in the Ad-S and the Ad-N₁ sections (Figs. 12C, 13), which
429 is unrealistic. On top of that, the $\delta^{13}\text{C}_{\text{org}}$ profile of the T_{DMD} is controversial because of
430 the following facts: (1) average $\delta^{13}\text{C}_{\text{org}}$ values of the alleged pre-PETM and PETM
431 segments of the Esplugafreda Formation only differ by ~ 0.7 ‰ (25.0‰ and 25.7‰,
432 respectively), a shift much smaller than the one expected for the CIE onset; (2) although
433 $\delta^{13}\text{C}_{\text{org}}$ values lower than -25‰, typical of the PETM, are dominant in the upper 8 m of

434 Esplugafreda Formation, similar values also occur in about half of the samples from the
435 pre-PETM interval; (3) given the proximity of the T_{DMD} and T_{dt} sections (Fig. 12A),
436 $\delta^{13}\text{C}_{\text{org}}$ values of their supposed PETM intervals should be similar but they do differ by
437 -1.1 ‰ on average, and the values of the latter (-24 to -25.2 ‰) match those of the pre-
438 PETM segment of the former (Figs. 12C, E, 13).

439 The reason why $\delta^{13}\text{C}_{\text{org}}$ values from the upper part of the Esplugafreda Formation in the
440 T_{DMD} and T_{dt} sections are more negative than in coeval deposits of the St Adria valley
441 still needs to be investigated. One possibility is that sediments from the T_{DMD} section
442 contain a high proportion of re-sedimented fossil carbon depleted in ^{13}C . In that case,
443 however, the isotopic composition of the 8 m interval of the Esplugafreda Formation
444 situated below the CC in the T_{DMD} and T_{dt} sections should be similar, which is not the
445 case. An alternative scenario could be that the $\delta^{13}\text{C}_{\text{org}}$ values of the samples collected in
446 the vegetated T_{DMD} ravine have been tainted by recent root traces, as hinted by the
447 uppermost sample collected from the vegetated part of the T_{dt} section. Whatever the
448 case, the above facts strongly suggest that the $\delta^{13}\text{C}_{\text{org}}$ profiles of the T_{DMD} and T_{dt}
449 sections do not faithfully record the global trend and, consequently, are not well suited
450 to fix the position of the CIE onset.

451 In the Claret sector the marked erosional character of the base of the CC
452 (Supplementary Fig. 3A) suggests also an encasement of the unit, but the total amount
453 of the erosion into the underlying deposits cannot be quantified. Therefore, the possible
454 preservation of the CIE onset in this sector can only be appraised through an inspection
455 of continuous isotopic profiles. Such an inspection cannot be carried out in the Claret
456 road section, since no samples can be retrieved from the 2-m-thick covered interval
457 below the CC (Figs. 7, 8, 13).

458 The Claret north and Claret hamlet sections, in which the boundary between the incised
459 valley fill and the CC is well exposed, offer a better chance (Figs. 6, 13). In the former,
460 pre-PETM $\delta_{13}\text{C}_{\text{org}}$ values (-22.0 to -22.9‰) persist in the grey calcarenites and marls
461 until 20 cm below the CC base, where a single value of -25.2‰ was obtained (Figs. 6A,
462 13). Should it mark the CIE isotope shift, the PETM onset would be situated just about
463 20 cm below the CC. However, the return to less negative $\delta_{13}\text{C}_{\text{org}}$ values higher up (-
464 24.2 to -22.3‰) argues against the -25.2‰ value as the initiation of a persistent shift.
465 Alternatively, this very negative value might be attributed to the recent alteration
466 observable in the sediments situated immediately below the CC (Supplementary Fig.
467 3A).

468 As explained before, the red mudstones of the Claret hamlet section are thought to
469 record the final infilling of the incised valley. If this interpretation proves correct, they
470 post-date the grey calcarenites and marls of the Claret north section. The four samples
471 analyzed from these red mudstones provided pre-PETM $\delta_{13}\text{C}_{\text{org}}$ values, from -24.4 to -
472 23.9‰ (-24.1‰ on average; Figs. 6B and 13). The $\delta_{13}\text{C}_{\text{carb}}$ values reported by Pujalte et
473 al. (2009) from three calcareous soil nodules from these red mudstones are also clearly
474 pre-PETM (-7.5‰; Supplementary Fig 3B). Therefore, no clear evidence of the CIE
475 onset can be discerned in any of the sections of the Claret sector.

476 *5.3. Sedimentary response to the PETM hydrological change*

477 Given that the development of extensive alluvial accumulations cannot be
478 instantaneous, some time must have elapsed from the onset of the PETM hydrological
479 change to the arrival of CC gravels and Yellowish Soils sediments to the study area, as
480 further demonstrated by the progradational character of the CC. The duration of the
481 delay was quantified by DMD (09-19) in 9–16 kyr in the Claret road section and in 13–

482 24 kyr in the T_{DMD} section, based on the CIE onset assumed in each of them. However,
483 according to the data discussed above, their assumption has been proven incorrect in the
484 former section and is highly uncertain in the latter.

485 The information obtained in this study offers the possibility to circumvent these two
486 problematic sections by focusing on the base of the Yellowish Soils in the sections in
487 which the CC is absent, rather than on the CC itself. In effect, based on Walther's Law
488 of Facies, it is reasonable to assume that the first Yellowish marls reached the study
489 area at approximately the same time as the CC, if not before.

490 The Ad-S and Ad-N₁ sections provide sound evidence that the onset of the CIE is
491 situated ~1m below the base of the Yellowish Soils (Figs. 10D, 11B). The exact
492 duration of this interval cannot be calculated with available methods and, therefore, it
493 has been tentatively estimated by assuming the same sedimentation rate as across the
494 PETM core. This procedure, although admittedly inexact, has the advantage of
495 permitting a direct comparison with the estimates of DMD (09-19).

496 The duration of the PETM onset and core was calculated in 80 kyr by Bowen et al.
497 (2004) and Röhl et al. (2007). In the Ad-S and Ad-N₁ sections the onset and core of the
498 PETM are represented by the topmost 1 m of the Esplugafreda Formation plus the 20 m
499 thick Yellowish Soils. Their 21 m cumulative thickness (compacted), therefore, implies
500 an average sedimentation rate of 26.25 cm kyr⁻¹. The 1 m thick segment of the PETM
501 onset preceding the accumulation of the Yellowish Soils to the study area consequently
502 represents ~3.8 kyr, less than half of the lowest estimate of DMD (09-19) and about one
503 sixth of their highest one. Interestingly, following a completely different approach,
504 Zeebe et al. (2016) calculated that the carbon release during the PETM onset lasted ~4
505 kyr, a similar figure to the one estimated herein.

506 Since the source area of the Garumnian alluvium was situated about 15 km to the north-
507 east from the study area (Supplementary Fig. 1) this figure entails an averaged
508 expansion rate of the extensive PETM depositional system of about 4 km/kyr. It is
509 unlikely, however, that such expansion rate was uniform throughout the ~3.8 kyr of the
510 CIE onset, since the shape of the initial isotope excursion clearly indicates a slow
511 increment of light carbon (Figs. 10D, 11B) and the climate response to warming is
512 slightly delayed (Zeebe et al., 2016). Also, both the temperature rise and the
513 concomitant increase of extreme rainfall episodes during the ongoing anthropogenic
514 warming of the Earth are being gradual (Shukla and Sen, 2021). Similar gradual
515 increases, therefore, may have occurred during the onset of the PETM. Consequently, it
516 is to be expected that the sedimentary expansion rate of the PETM alluvial system may
517 have been slow at first and progressively accelerated in parallel with the CO₂ emission
518 and the intensification of the warming. Whatever the case, the response of the
519 sedimentary system to the PETM hydrological change seems to have been, in geological
520 terms, comparatively rapid.

521 **6. Conclusions**

522 The claim that the sedimentary response to the PETM hydrological change in the south
523 Pyrenean Tresp-Graus Basin was delayed by 16.5 ± 7.5 kyr is challenged with new field
524 and organic carbon isotope data. This claim was based on the assertion that the onset of
525 the CIE was recorded 3 and 8 m below the CC in the Claret and Tendrui sections.
526 However, new field data and organic carbon isotopic analyses of one hundred samples
527 from eight sections, including the two conflicting ones, lead to a different conclusion.
528 Field mapping and observations demonstrate that at Claret, Tendrui and elsewhere in
529 the study area, the CC is erosively encased within the underlying deposits and is
530 laterally discontinuous. In two sections in which the CC is absent and the Yellowish

531 Soils conformably rest on the Esplugafreda Formation, coded Ad-S and Ad-N₁, the
532 onset of the CIE has been confidently pinpointed about 1 m below the base of the
533 Yellowish Soils. This onset, however, is truncated by the CC erosional base at the
534 Claret and Tendrui sections, making them unsuitable for any chronological
535 reconstructions.

536 As the expansion of alluvial systems cannot be instantaneous, some time must have
537 elapsed between the onset of the hydrological change and the arrival of PETM alluvium
538 to the study area. In fact, the internal architecture of the CC, indicative of intermittent
539 progradation, entails a progressive development. A tentative estimate, based on
540 sedimentation rates, suggests that the arrival of PETM alluvium to the Claret-Tendrui
541 area occurred ~3.8 kyr, after the onset of the CIE, about a third of the lowest estimate of
542 previous authors. Since the study area was situated about 15 km from the source area,
543 this new estimate entails a minimum expansion rate of about 4 km kyr⁻¹ and supports a
544 rapid environmental response of the sedimentary system to the PETM hydrological
545 change.

546 **Acknowledgements**

547 Research by VP and AP was supported by MINECO/MCI/FEDER-UE projects
548 CGL2015-65404-R and PID2019-105670GB-I00/AEI/10.13039/501100011033 of the
549 Spanish Government, and by the Consolidated Research Group IT930-16 of the Basque
550 Government. Research by BS was supported by the Swedish Research Council.

551 **References**

552 Allen, P. A., 2017. The sediment routing systems: the fate of sediments from source to
553 sink. Cambridge University Press, 403 pp.

554 Armitage, J. J., Duller, R. A., Whittaker, A.C., Allen P. A., 2011. Transformation of
555 tectonic and climatic signals from source to sedimentary archive. *Nat. Geosci* 4,
556 231–235 doi:10.1038/ngeo1087.

557 Armitage, J. J., Dunkley Jones, T., Duller, R. A., Whittaker, A. C., Allen, P. A., 2013.
558 Temporal buffering of climate-driven sediment flux cycles by transient catchment
559 response, *Earth and Planetary Science Letters*, 369–370, 200–210, doi:
560 10.1016/j.epsl.2013.03.020, 2013.

561 Baceta, J., Pujalte, V., Wright, V.P., Schmitz, B., 2011. Carbonate platform models,
562 sea-level changes and extreme climatic events during the Paleocene-early Eocene
563 greenhouse interval: a basin-platform-coastal plain transect across the southern
564 Pyrenean basin. In: *Pre-Meeting Field trips Guidebook, 28th IAS Meeting.*
565 Zaragoza (C. Arenas, L. Pomar and F. Colombo, Eds.). *Sociedad Geológica de*
566 *España, Geo-Guías*, 7:151-198.

567 Baczynski, A. A., McInerney, F. A., Freeman, K. H., Wing, S. L., & the Bighorn Basin
568 Coring Project (BBCP) Science Team (2019). Carbon isotope record of trace
569 n-alkanes in a continental PETM section recovered by the Bighorn Basin Coring
570 Project (BBCP). *Paleoceanography and Paleoclimatology*, 34, 1–13.
571 <https://doi.org/10.1029/2019PA003579>

572 Baczynski, A.A., McInerney, F.A., Wing, S.L., Kraus, M.J., Bloch, J.I., Boyer, D.M.,
573 Secord, R., Morse, P.E., Fricke, H.C., 2013. Chemostratigraphic implications of
574 spatial variation in the Paleocene-Eocene Thermal Maximum carbon isotope
575 excursion, SE Bighorn Basin, Wyoming. *Geochem. Geophys.* 14, 4133–4152. doi:
576 10.1002/ggge.20265.

577 Baczynski, A.A., McInerney, F.A., Wing, S.L., Kraus, M.J., Morse, P.E., Bloch, J. I.,
578 Chung, A. H., Freeman, K. H., 2016. Distortion of carbon isotope excursion in bulk
579 soil organic matter during the Paleocene-Eocene thermal maximum. *GSA Bulletin*,
580 128, 1352–1366. doi:10.1130/B31389.1

581 Bowen, G.J., Beerling, D.J., Koch, P.L., Zachos, J.C., and Quattlebaum, T., 2004, A
582 humid climate state during the Palaeocene-Eocene thermal maximum: *Nature*, v.
583 432, p. 495–499, doi:10.1038/nature03115.

584 Capel Molina, J., 1974. Génesis de las inundaciones de Octubre de 1973 en el Sureste
585 de la Península Ibérica. *Cuad. Geog.*, 4, 140–166

586 Carmichael, M. J., Inglis, G. N., Badger, M. P. S., Naafs, D. A., Behrooza, L.,
587 Remmelzwaal, S., Monteiro, F. M., Rohrssen, M., Farnsworth, A., Buss, H. L.,
588 Dickson, A. J., Valdes, P.J., Lunt, D. J., Pancost, R. D., 2017. Hydrological and
589 associated biogeochemical consequences of rapid global warming during the
590 Paleocene-Eocene Thermal Maximum. *Gloplacha*, 157, 114–138.
591 <https://doi.org/10.1016/j.gloplacha.2017.07.014>

592 Carmichael, M. J., Pancost, R. D., Lunt, D. J., 2018. Changes in the occurrence of
593 extreme precipitation events at the Paleocene–Eocene thermal maximum. *Earth*
594 *Planet. Sci. Lett.* 501, 24–36. <https://doi.org/10.1016/j.epsl.2018.08.005>

595 Colombera, L., Arévalo, O. J., Mountney, N. P., 2017. Fluvial-system response to
596 climate change: The Paleocene-Eocene Tresp Group, Pyrenees, Spain. *Gloplacha*
597 157, 1–17. <https://doi.org/10.1016/j.gloplacha.2017.08.011>

598 Cuevas, J.L., 1992. Estratigrafía del “Garumniense” de la Conca de Tresp. *Prepirineo*
599 de Lérida. *Acta Geol. Hisp.* 27, 95–108.

600 Deser, C., Lehner, F., Rodgers, K.B., Ault, T., Delworth, T.L., DiNezio, P.N., Fiore, A.,
601 Frankignoul, C., Fyfe, J.C., Horton, D.E., Kay, J.E., Knutti, R., Lovenduski, N.S.,
602 Marotzke, J., McKinnon, K.A., Minobe, S., Randerson, J., Screen, J.A., Simpson
603 I.R., Ting, M., 2020. Insights from Earth system model initial-condition large
604 ensembles and future prospects. *Nat. Clim. Chang.* 10, 277–286
605 <https://doi.org/10.1038/s41558-020-0731-2>

606 Domingo, L., López-Martínez, N., Leng, M. J., Grimes, S.T., 2009. The Paleocene–
607 Eocene Thermal Maximum record in the organic matter of the Claret and Tendrúy
608 continental sections (South-central Pyrenees, Lleida, Spain). *Earth Planet. Sci. Lett.*
609 281, 226–237. <https://doi.org/10.1016/j.epsl.2009.02.025>

610 Duller, R.A., Armitage, J.J., Hayley R. Manners, H.R., Grimes, S., Dunkley Jones, J.,
611 2019. Delayed sedimentary response to abrupt climate change at the Paleocene-
612 Eocene boundary, northern Spain. *Geology* 47, 159–162,
613 <https://doi.org/10.1130/G45631.1>

614 Foreman, B.Z., 2014. Climate-driven generation of a fluvial sheet sand body at the
615 Paleocene-Eocene boundary in north-west Wyoming (USA). *Basin Res.* 26, 225–
616 241. <https://doi.org/10.1111/bre.12027>

617 Foreman, B.Z., Heller, P. L., Clementz, M. T., 2012. Fluvial response to abrupt global
618 warming at the Palaeocene/Eocene boundary. *Nature* 491, 92–95.
619 <https://doi.org/10.1038/nature11513>

620 García Veigas, J., 1997. First Continental
621 Evaporitic Phase in the South Pyrenean Central Area: Tresp Gypsum (Garumn
622 Facies, Upper Paleocene; Allochthonous Zone). In: Busson, G., Schreiber, B.Ch.
623 (Eds.), *Sedimentary Deposition in Rift and Foreland Basins in France and Spain*
(Paleogene and Lower Neogene). Columbia University Press, pp. 335–342.

624 García Veigas, J., 1997. First Continental Evaporitic Phase in the South Pyrenean
625 Central Area: Tresp Gypsum (Garumn Facies, Upper Paleocene; Allochthonous
626 Zone). In: Busson, G., Schreiber, B.Ch. (Eds.), *Sedimentary Deposition in Rift and*
627 *Foreland Basins in France and Spain (Paleogene and Lower Neogene)*. Columbia
628 University Press, pp. 335–342.

629 Gibson, T. G., Bybell, L. M., Mason, D. B., 2000. Stratigraphic and climatic
630 implications of clay mineral changes around the Paleocene/Eocene boundary of the
631 northeastern US margin. *Sedim. Geol.* 134, 65–92. [https://doi.org/10.1016/S0037-](https://doi.org/10.1016/S0037-0738(00)00014-2)
632 [0738\(00\)00014-2](https://doi.org/10.1016/S0037-0738(00)00014-2)

633 Handley, L., O’Halloran, A., Pearson, P. N., Hawkins, E., Nicholas, C.J., Schouten, S.,
634 McMillan, I. K., Pancost, R. D., 2012. Changes in the hydrological cycle in trop-
635 ical East Africa during the Paleocene-Eocene Thermal Maximum. *Palaeogeogr.*
636 *Palaeoclimatol. Palaeoecol.* 329,10–21,
637 <http://dx.doi.org/10.1016/j.palaeo.2012.02.002>.

638 Held. I.M., Soden B.J., (2006) Robust Responses of the Hydrological Cycle to Global
639 Warming. *J. Clim.* 19, 5686–5699. <https://doi.org/10.1175/JCLI3990.1>

640 Hernández-Molina, F. J., Somoza, L., Vázquez, J. T., Rey, J. 1995. Estructuración de
641 los prismas litorales del Cabo de Gata: respuesta a los cambios climático-eustáticos
642 holocenos. *Geogaceta*, 18, 79–82

643 Jiang, J., Hu, X., Li, J., BouDagher-Fadel, M., Garzanti, E., 2021. Enhanced
644 hydrological change during the Paleocene-Eocene thermal maximum (PETM)
645 recorded in shallow-marine Xigaze forearc basin (southern Tibet). *Palaeogeogr.*
646 *Palaeoclimatol. Palaeoecol.* 562 (2021), 110095.
647 <https://doi.org/10.1016/j.palaeo.2020.110095>

648 John, C.M., Bohaty, S.M., Zachos, J.C., Sluijs, A., Gibbs, S., Brinkhuis, H., Bralower,
649 T.J., 2008. North American continental margin records of the Paleocene–Eocene
650 thermal maximum: implications for global carbon and hydrological cycling.
651 *Paleoceanography* 23, PA2217. doi:10.1029/2007PA001465

652 Koch, P.L., Zachos, J.C., Gingerich, P.D., 1992. Correlation between isotope records in
653 marine and continental carbon reservoirs near the Paleocene/Eocene boundary.
654 *Nature* 358, 319–322.

655 Kraus, M. J., McInerney, F. A., Wing, S. L., Secord, R., Baczynski, A. A., Bloch, J. I.,
656 2013. Paleohydrologic response to continental warming during the Paleocene–
657 Eocene Thermal Maximum, Bighorn Basin, Wyoming. *Palaeogeogr.*
658 *Palaeoclimatol. Palaeoecol.* 370, 196–208. doi: 10.1016/j.palaeo.2012.12.008

659 Kraus, M.J., Woody, D.T., Smith, J.J., Dukic, V., 2015. Alluvial response to the
660 Paleocene–Eocene Thermal Maximum climatic event, Polecat Bench, Wyoming
661 (U.S.A.). *Palaeogeogr. Palaeoclimatol. Palaeoecol.* 435, 177–192.
662 <https://doi.org/10.1016/j.palaeo.2015.06.021>

663 Manners, H.R., Grimes, S.T., Sutton, P.A., Domingo, L., Leng, M.J., Twitchett, R.J.,
664 Hart, M.B., Dunkley Jones, T., Pancost, R.D., Duller, R., Lopez-Martinez, N.,
665 2013. Magnitude and profile of organic carbon isotope records from the Paleocene–
666 Eocene Thermal Maximum: evidence from northern Spain. *Earth Planet. Sci. Lett.*
667 376, 220–230. <http://dx.doi.org/10.1016/j.epsl.2013.06.016>

668 Maufrangeas, A., Leleu, S., Loisy, C., Roperch, P., Jolley, D., Vinciguerra C., Nguyen-
669 Thuyet, O., 2020. Stratigraphy of the Paleocene continental sedimentary succession
670 of the northern Pyrenean basin (Corbières, southern France) using $\delta^{13}\text{C}_{\text{org}}$ isotopes.
671 *J. Geol. Soc. London*, 177, 752–765, <https://doi.org/10.1144/jgs2019-084>

672 McInerney, F.A., Wing, S.L., 2011. The Paleocene Eocene ThermalMaximum: a
673 perturbation of carbon cycle, climate, and biosphere with implications for the
674 future. *Annu. Rev. Earth Planet. Sci* 39, 489–516. DOI: 10.1146/annurev-earth-
675 040610-133431

676 Minelli, N., Manzi, V., Roveri, M. 2013. The record of the Paleocene-Eocene thermal
677 maximum in the Ager Basin (Central Pyrenees, Spain). *Geol. Acta*, 11, 421–441.
678 DOI: 10.1344/105.000002061

679 Pancost, R.D., 2017. Climate change narratives. *Nature Geoscience*, 10, 466–468.

680 Payros, A., Pujalte, V., Orue-Etxebarria, X., Apellaniz, E., Bernaola, G., Baceta, J.I.,
681 Caballero, F., Dinarés-Turell, J., Monechi, S., Ortiz, S., Schmitz, B., Tosquella, J.,
682 2016. The Relevance of Iberian Sedimentary Successions for Paleogene
683 Stratigraphy and Timescales. In: Montenari, M. (Ed.), *Stratigraphy & Timescales*,
684 pp. 393–489.

685 Plink-Björklund P., Birgeneier L., Jones E, 2014. Extremely bad early Eocene weather:
686 Evidence for extreme precipitation from rived deposits. *Rendiconti Online della*
687 *Soc. Geol. It.* 31, 175–176. doi: 10.3301/ROL.2014.107

688 Pujalte, V., Baceta, J.I., Schmitz, B., Orue-Etxebarria, X., Payros, A., Bernaola, G.,
689 Apellaniz, E., Caballero, F., Serra-Kiel, J., Tosquella, J., 2009. Redefinition of the
690 Ilerdian Stage (early Eocene). *Geol. Acta* 7, 177–194.
691 <https://doi.org/10.1344/105.000000268>

692 Pujalte, V., Robador, A., A., Samsó, J.M^a. 2016. A siliciclastic braid delta within a
693 lower Paleogene carbonate platform (Ordesa-Monte Perdido National Park,
694 southern Pyrenees, Spain): Record of the Paleocene–Eocene Thermal Maximum

695 perturbation. *Palaeogeogr. Palaeoclimatol. Palaeoecol.*, 459, 453–470.
696 <http://dx.doi.org/10.1016/j.palaeo.2016.07.029>

697 Pujalte, V., Schmitz, B., 2005. Revisión de la estratigrafía del Grupo Tremp
698 (“Garumniense”, Cuenca de Tremp-Graus, Pirineos meridionales). *Geogaceta* 38,
699 79–82.

700 Pujalte, V., Schmitz, B., 2014. Comment on “Magnitude and profile of organic carbon
701 isotope records from the Paleocene–Eocene Thermal Maximum: evidence from
702 northern Spain” by Manners et al. [*Earth Planet. Sci. Lett.* 376 (2013) 220–230].
703 *Earth Planet. Sci. Lett.* 395, 291–293. <https://doi.org/10.1016/j.epsl.2014.03.054>

704 Pujalte, V., Schmitz, B., 2019. Record of the Paleocene–Eocene Thermal Maximum in
705 the Southern and Western Pyrenees. In: C. Quesada and J. T. Oliveira (eds.), *The*
706 *Geology of Iberia: A Geodynamic Approach*, Springer Nature Switzerland AG. pp.
707 13–17. https://doi.org/10.1007/978-3-030-11190-8_2.

708 Pujalte, V., Schmitz, B., Baceta, J.I., 2014. Sea-level changes across the Paleocene–
709 Eocene interval in the Spanish Pyrenees, and their possible relationship with North
710 Atlantic magmatism. *Palaeogeogr. Palaeoclimatol. Palaeoecol.* 393, 45–60.
711 <https://doi.org/10.1016/j.palaeo.2013.10.016>

712 Röhl, U., Westerhold, T., Bralower, T.J., Zachos, J.C., 2007. On the duration of the
713 Paleocene- Eocene Thermal Maximum (PETM). *Geochem. Geophys. Geosyst.* 8, 1-
714 13. <https://doi.org/10.1029/2007GC001784>.

715 Rosell, J., Linares, R., Llompart, C., 2001. El “Garumniense” prepirenaico. *Rev. Soc.*
716 *Geol. Esp.* 14, 47–56.

717 Schmitz, B., Pujalte, V., 2003. Sea-level, humidity, and land-erosion records across the
718 initial Eocene thermal maximum from a continental-marine transect in northern
719 Spain. *Geology* 31, 689–692. doi:<https://doi.org/10.1130/G19527.1>

720 Schmitz, B., Pujalte, V., 2007. Abrupt increase in seasonal extreme precipitation at the
721 Paleocene-Eocene boundary. *Geology* 35, 215–218.
722 doi:<https://doi.org/10.1130/G23261A.1>

723 Schmitz, B., Pujalte, V., Núñez-Betelu, K., 2001. Climate and sea-level perturbations
724 during the Incipient Eocene Thermal Maximum: evidence from siliciclastic units in
725 the Basque Basin (Ermua, Zumaia and Trabakua Pass), northern Spain.
726 *Palaeogeogr. Palaeoclimatol. Palaeoecol.*, 165, 299–320.
727 [https://doi.org/10.1016/S0031-0182\(00\)00167-X](https://doi.org/10.1016/S0031-0182(00)00167-X)

728 Shukla, T. and Sen, I. S., 2021. Preparing for floods on the Third Pole. *Science* 372,
729 232–234. DOI: 10.1126/science.abh3558

730 Simpson, G., Castellort, S., 2012. Model shows that rivers transmit high-frequency
731 climate cycles to the sedimentary record. *Geology* 40, 1131–1134.
732 doi:<https://doi.org/10.1130/G33513.1>

733 Slotnick, B.S., Dickens, G.R., Nicolo, M.J., Hollis, C.J., Crampton, J.S., Zachos, J.C.,
734 Sluijs, A., 2012. Large-amplitude variations in carbon cycling and terrestrial
735 weathering during the Latest Paleocene and Earliest Eocene: the record at Mead
736 Stream, New Zealand. *J. Geol* 120, 487–505. DOI: 10.1086/666743

737 Sluijs, A., Bowen, G.J., Brinkhuis, H.L., Lourens, J., Thomas, E., 2007. The
738 Palaeocene–Eocene ThermalMaximum super greenhouse: biotic and geochemical
739 signatures, age models and mechanisms of global change. In: Williams, M.,
740 Haywood, A.M., Gregory, F.J., Schmidt, D.N. (Eds.), *Deep-Time Perspectives on*

741 Climate Change: Marrying the Signal from Computer Models and Biological
742 Proxies. Special Publications, The Geological Society, London, The
743 Micropalaeontological Society, pp. 323–349.

744 Storme, J.-Y., Devleeschouwer, X., Schnyder, J., Cambier, G., Baceta, J.I., Pujalte, V.,
745 Di Matteo, A., Iacumin, P., and Yans, J, 2012. The Palaeocene/Eocene boundary
746 section at Zumaia (Basque-Cantabric Basin) revisited: new insights from high-
747 resolution magnetic susceptibility and carbon isotope chemostratigraphy on organic
748 matter ($\delta^{13}\text{C}_{\text{org}}$), *Terra Nova*, 24, 310–317. doi: 10.1111/j.1365-3121.2012.01064.x

749 Yans, J., Marandat, B., Masure, E., Serra-Kiel, J., Schnyder, J., Storme J.-Y., Marivaux,
750 L., Adnet, S., Vianey-Liaud, M., Rodolphe Tabuce, R., 2014. Refined bio- (benthic
751 foraminifera, dinoflagellate cysts) and chemostratigraphy ($\delta^{13}\text{C}_{\text{org}}$) of the earliest
752 Eocene at Albas-Le Clot (Corbières, France): implications for mammalian
753 biochronology in Southern Europe. *Newsl Stratigr.* 47 331–353. DOI:
754 10.1127/nos/2014/0050

755 Zachos, J. C.; Dickens, G. R.; and Zeebe, R. E. 2008. An early Cenozoic perspective on
756 greenhouse warming and carbon-cycle dynamics. *Nature* 451 279–283. DOI:
757 10.1038/nature06588.

758

759 **Figure Captions**

760 Fig. 1. Abrupt expansion (~270 m) of a small fan delta in the semiarid southeast coast of
761 peninsular Spain during a single major flood (2,580 m³/seg at peak flow) after two days
762 of heavy rain in October 1973.

763 Fig. 2. (A) Simplified early Paleogene palaeogeography of the Pyrenean domain. (B)
764 Outcrop map of the east part of the Tremp-Graus Basin with location of the study area.

765 (C) Outcrop map of the Paleocene-Eocene interval in the study area. (D) Simplified S-N
766 section (projected) showing the location of sections and outcrops described in the text
767 (vertical scale exaggerated).

768 Fig. 3. Incised valley grey-coloured deposits at the Claret road section. (A) General
769 view. (B) Close-up of the imbricated basal conglomerates of the valley fill. (C) Buried
770 tree trunk in living position. (D) Abundant coal remains in a sample of the incised
771 valley calcarenites.

772 Fig. 4. (A) Incised valley red calcareous mudstones directly overlain by the Claret
773 Conglomerate. (B) Close-up of the altered zone of the red mudstones directly below the
774 Claret Conglomerate.

775 Fig. 5. (A) Outcrop map of the Paleocene-Eocene boundary deposits in the Claret sector
776 with indication of palaeocurrents and location of the Claret north section (illustrated in
777 B) and the Palau creek section (illustrated in C).

778 Fig. 6. Close up views and $\delta^{13}\text{C}_{\text{org}}$ values from the topmost part of the incised valley fill
779 deposits of the Claret north (A) and the Claret hamlet (B) sections. Explanation within
780 the text.

781 Fig. 7. (A) Map of the base and top of the CC drawn on a Google Earth satellite image
782 of the area surrounding the Claret road section. Note that the CC base is hidden by
783 vegetation throughout. (B, C) Field view and sketch of the upper part of the incised
784 valley deposits, the poorly exposed CC and the intervening covered interval (location in
785 A). Values of $\delta^{13}\text{C}_{\text{org}}$ isotopes from incised valley deposits are indicated in the sketch.

786 Fig. 8. (A) Sketch of the CC in the Claret road section, drawn from field photos B–D.
787 As the outcrop is situated on a road bend, the perspective of the successive photos is

788 distorted. To alleviate the distortion, two characteristic points are marked in different
789 pictures: a small yellow circle in B and C, and a circled fallen block (arrowed) in A, C
790 and D. The orange line (in the online version) marks the base of the same conglomeratic
791 bed in all pictures. $\delta^{13}\text{C}_{\text{org}}$ values from marly clays are shown in A.

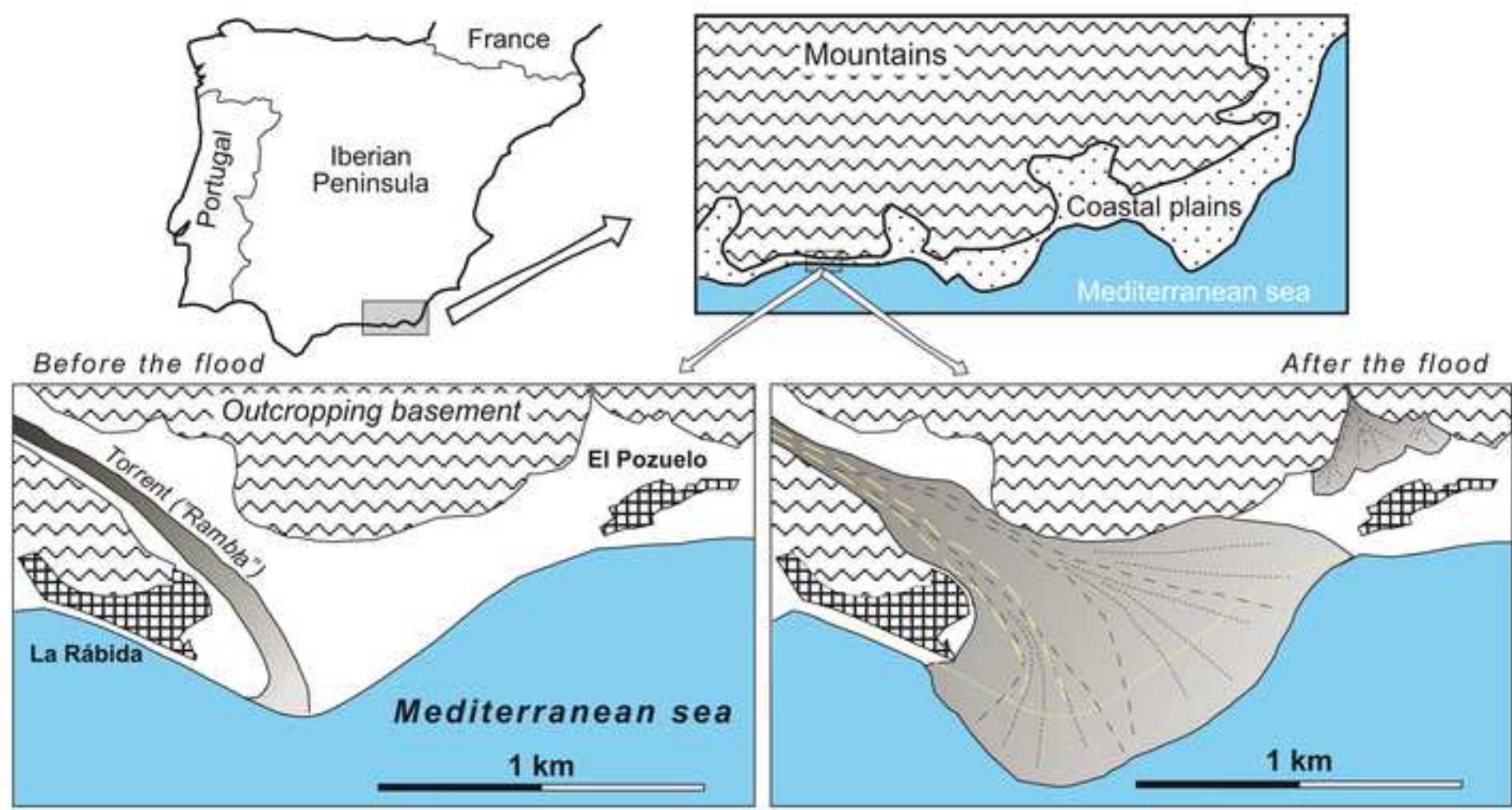
792 Fig. 9. (A) Close-up of the upper part of the Ad-S section. (B) Micrographs of a thin
793 section of a purple cap sample illustrating two of its numerous ferruginous nodules.

794 Fig. 10. (A, B) Field views of two adjacent segments of the southern margin of the St
795 Adria valley illustrating the encasement of the CC into the Esplugafreda Formation
796 (location in Fig. 2C). (C) General view of the Ad-S section (location in A and B). (D)
797 $\delta^{13}\text{C}_{\text{org}}$ isotopic profile of the Ad-S section. (E) Field view of a calcarenite channel with
798 its base party eroding the Esplugafreda Formation (location in B).

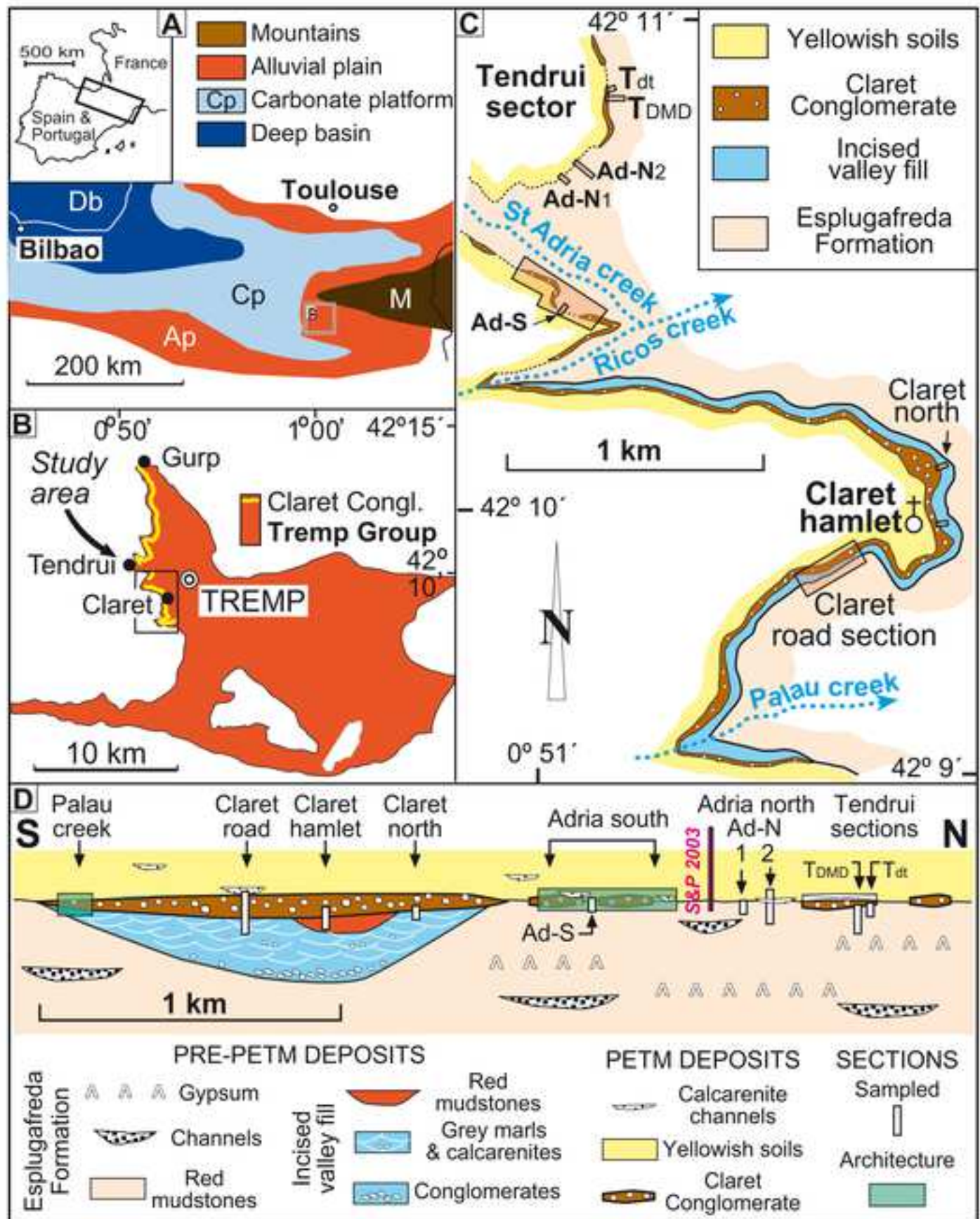
799 Fig. 11. (A) Field view of the northern margin of the St Adria valley and southern part
800 of the Tendrui sector showing the location of the Ad-N₁ and Ad-N₂ sections, the tree-
801 covered CC of the Tendrui sector and the farm-land situated just above it. (B) Field
802 view and isotope profile of the Ad-N₁ section. The encircled hammer in the photo is
803 situated on the purple cap. (C) Close-up of the Esplugafreda Formation red marls in the
804 Ad-N₁ section showing its numerous CaCO₃ soil nodules (some encircled). (D) $\delta^{13}\text{C}_{\text{org}}$
805 isotope profile of the Ad-N₂ section.

806 Fig. 12. (A) Field view of the northern part of the Tendrui sector with location of the
807 T_{DMD} and the T_{dt} sections. Note abundant vegetation. (B, C) Field view and isotope
808 profile of the T_{DMD} section. (D, E) Field view and isotope profile of the T_{dt} section.

809 Fig. 13. Organic carbon isotope profiles from the P-E boundary sections analyzed in this
810 study. Note that values of the T_{DMD} section are at odds with those of the other sections.
811 Explanation within the text.



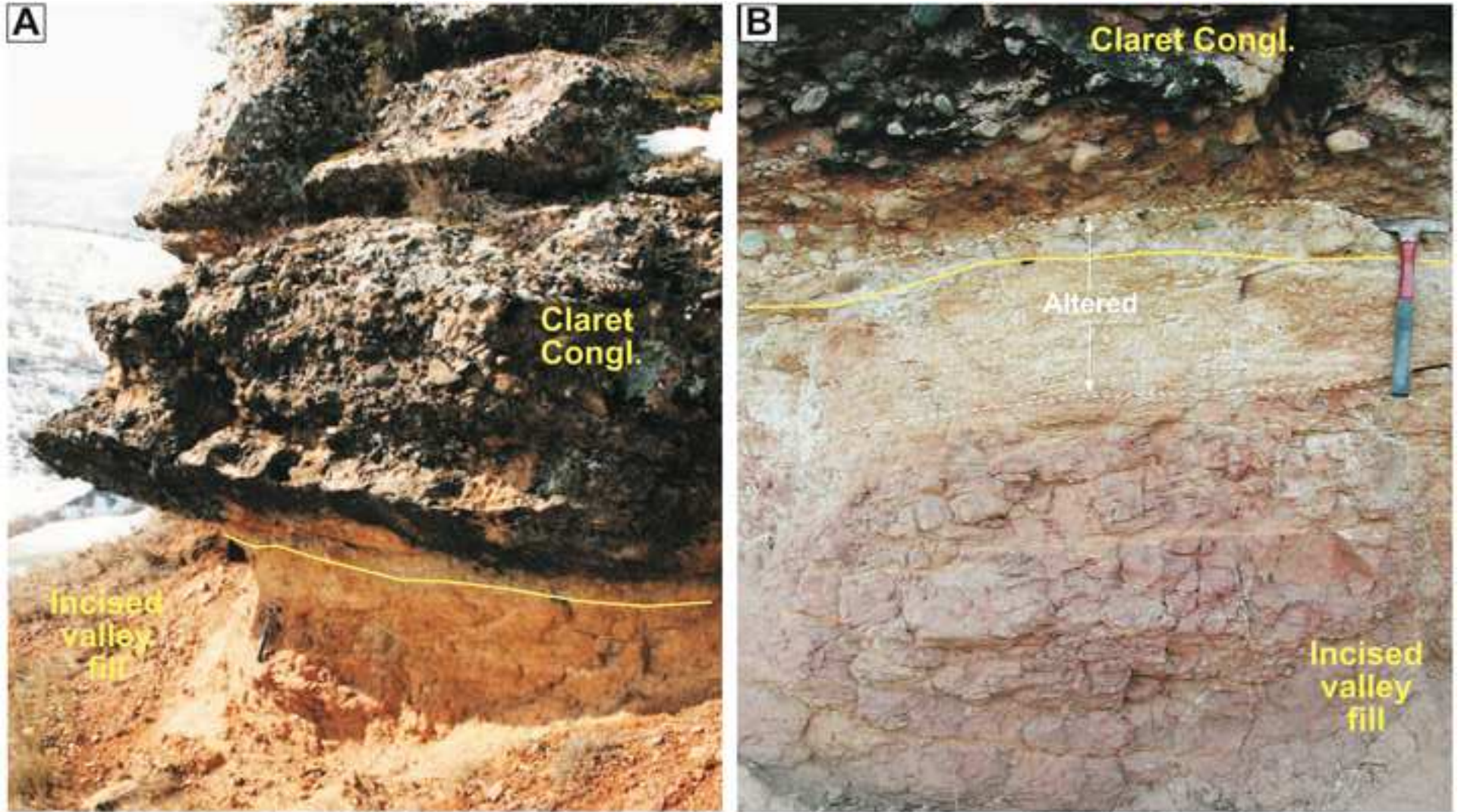
Pujalte et al Fig 1



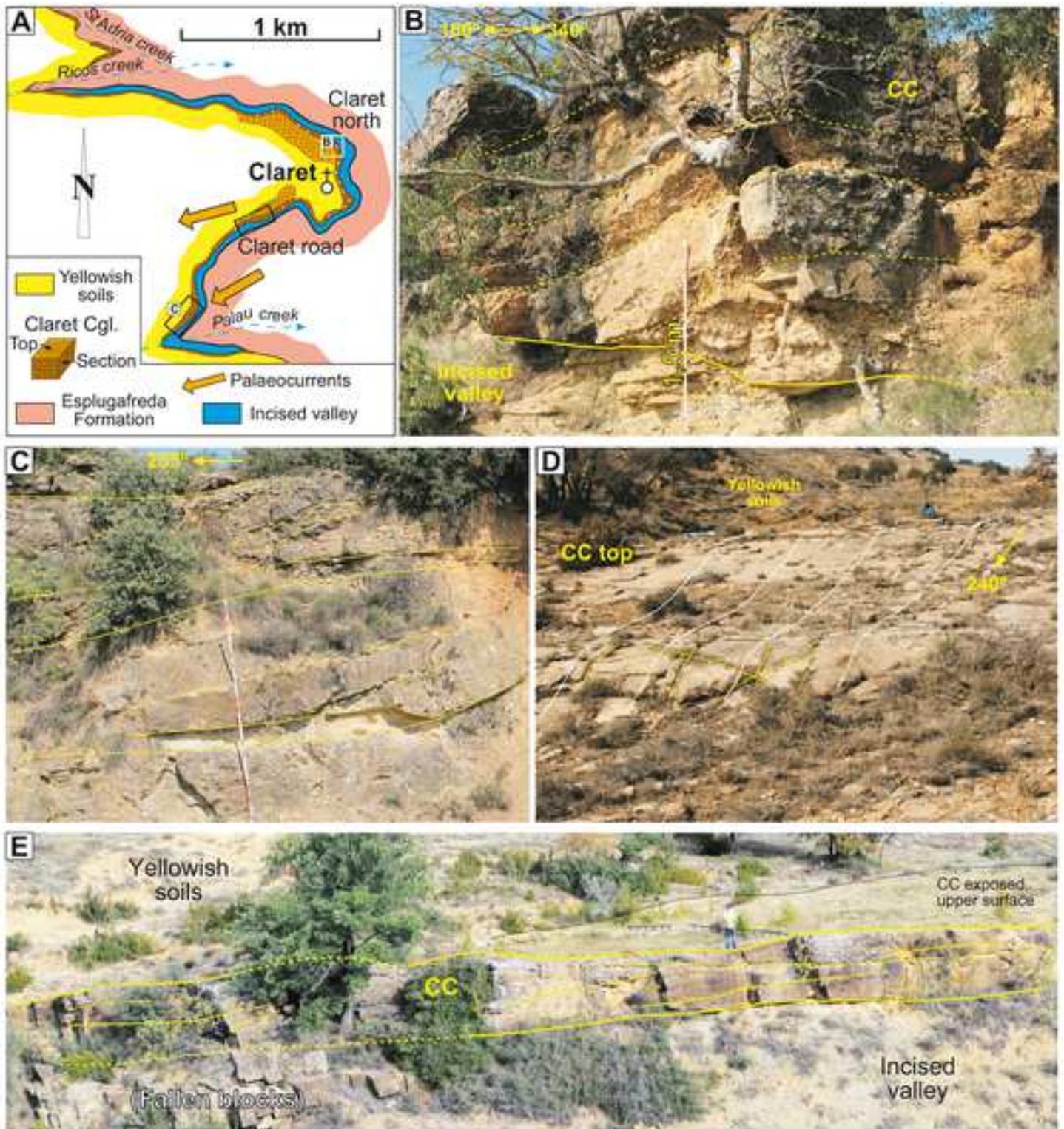
Pujalte et al Fig 2



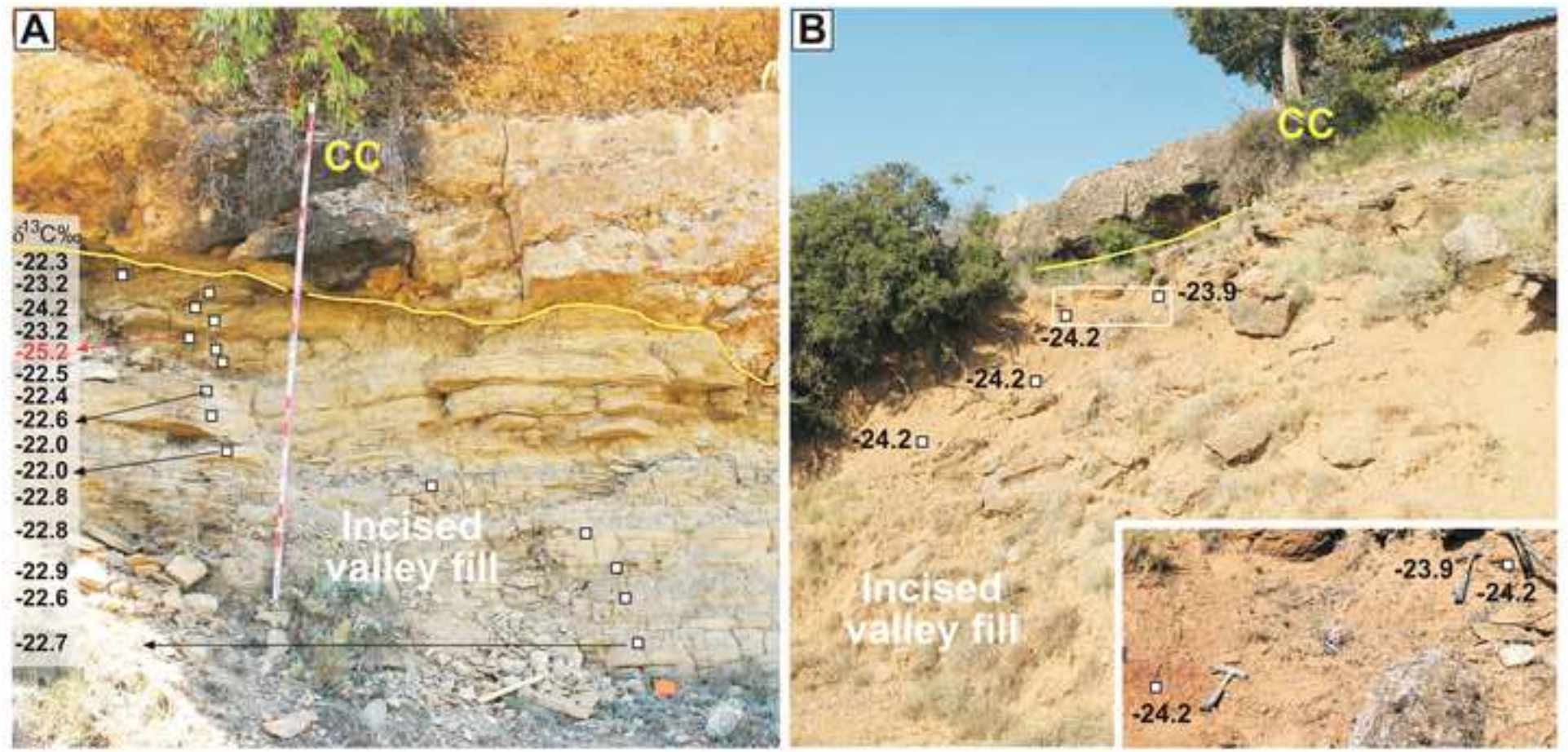
Pujalte et al Fig 3



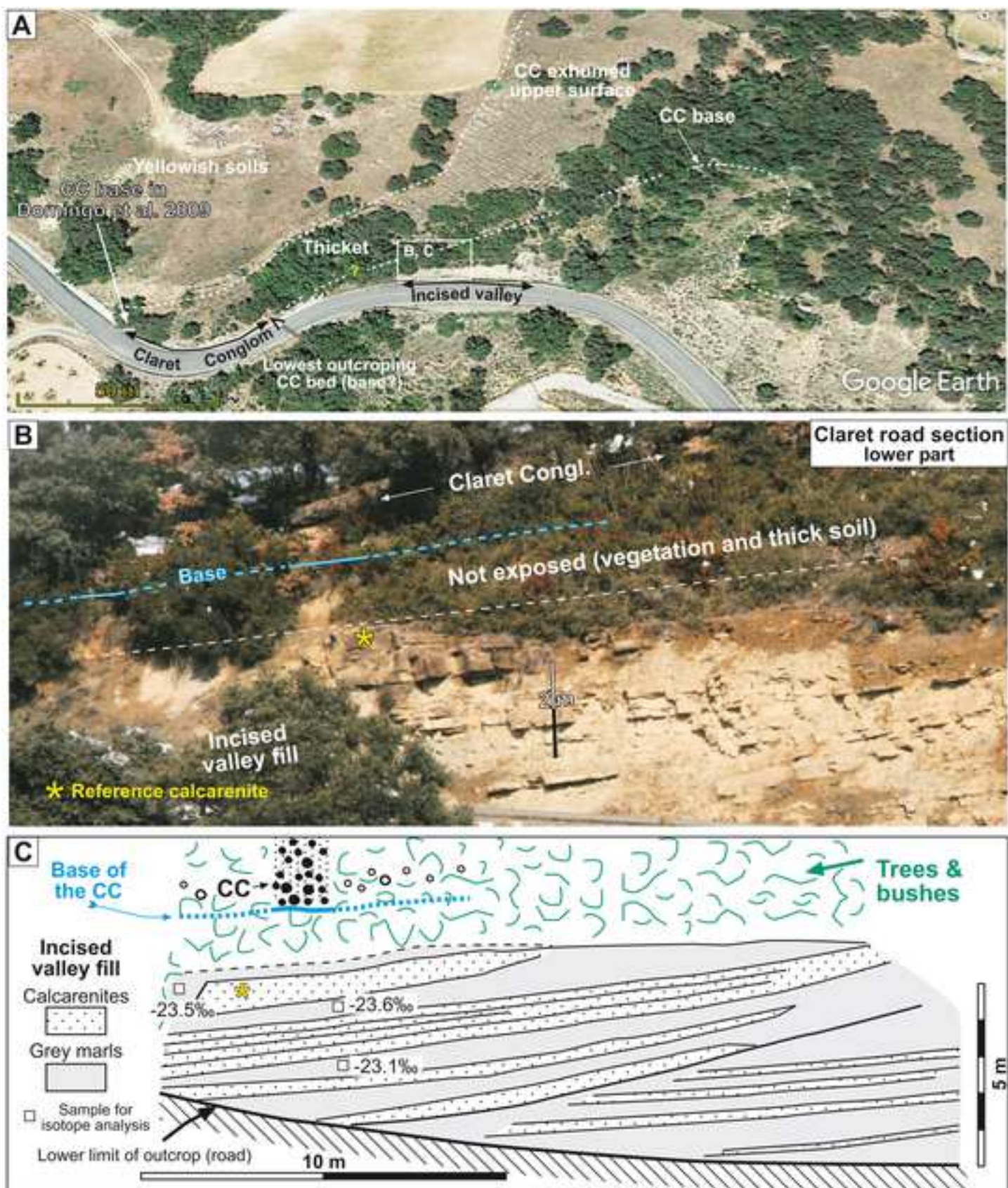
Pujalte et al Fig 4



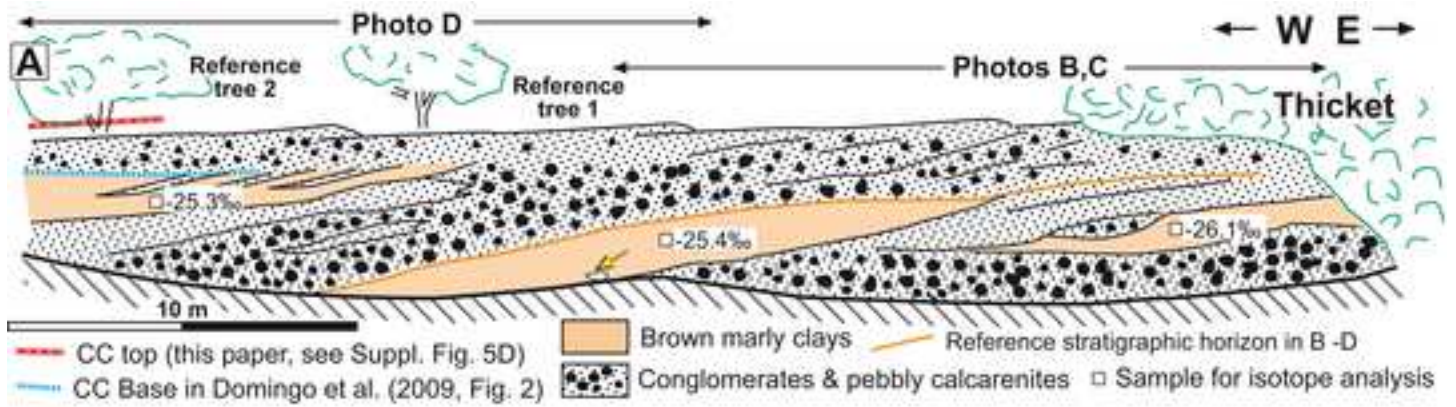
Pujalte et al Fig 5



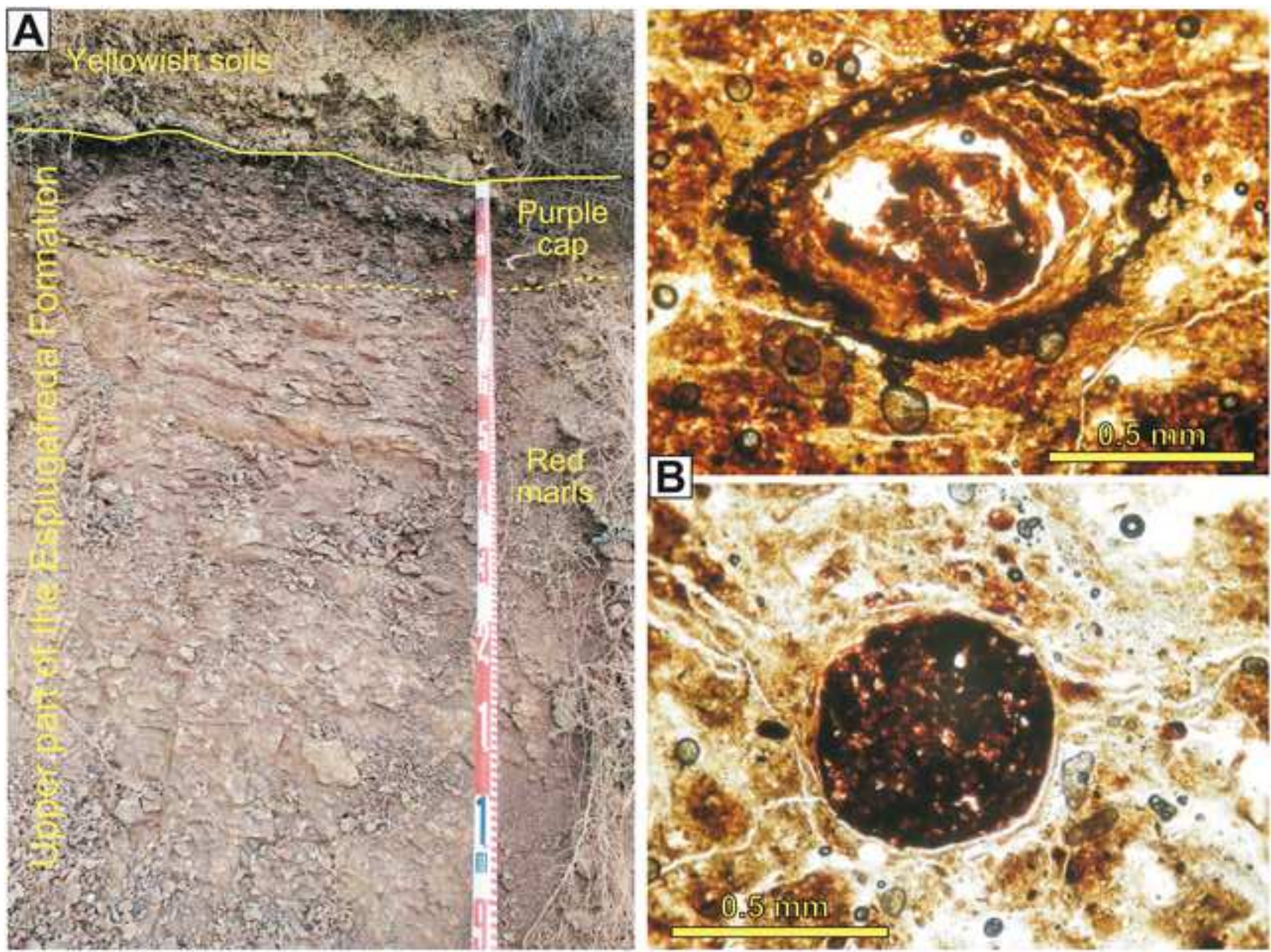
Pujalte et al Fig 6



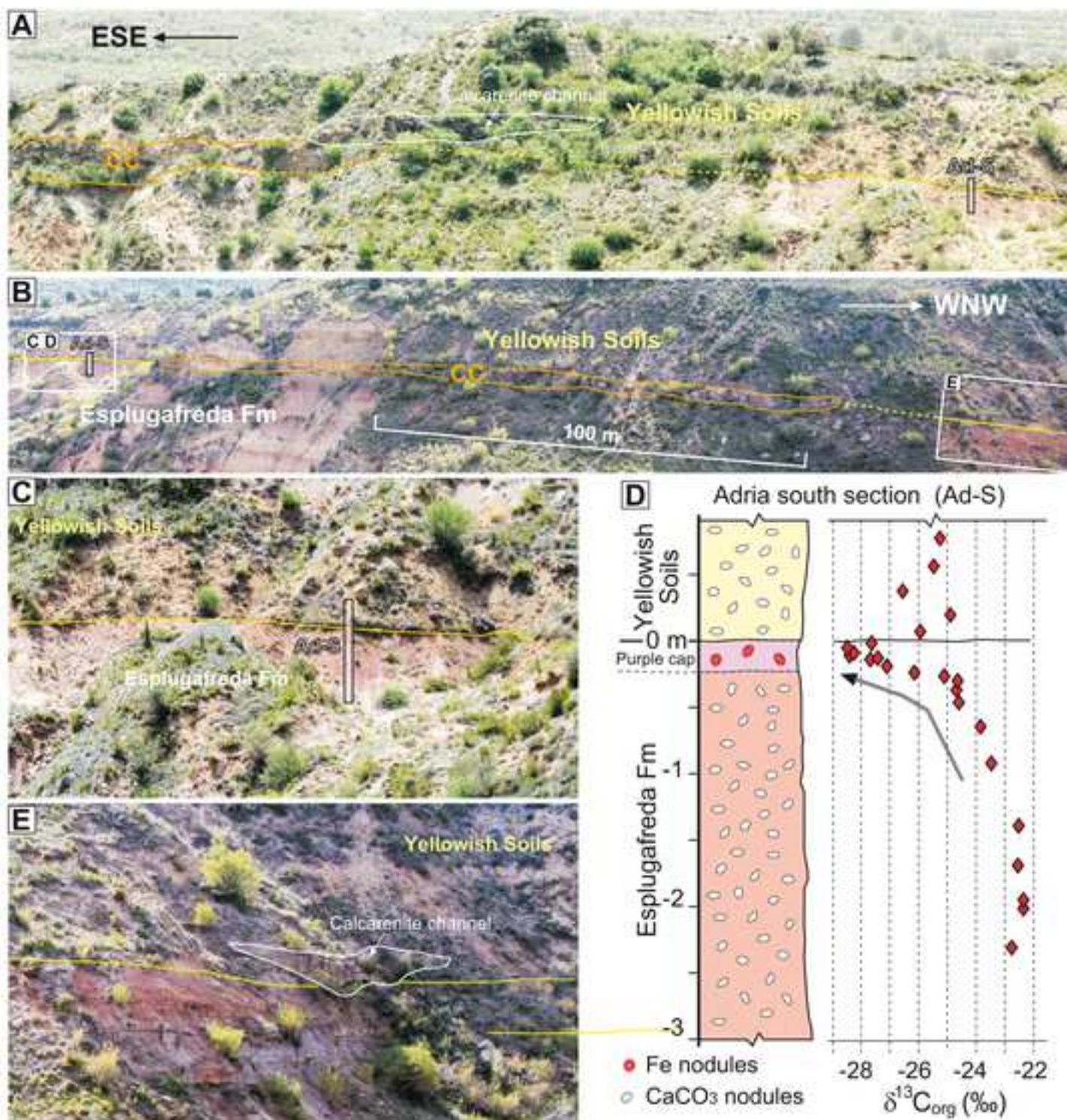
Pujalte et al Fig 7



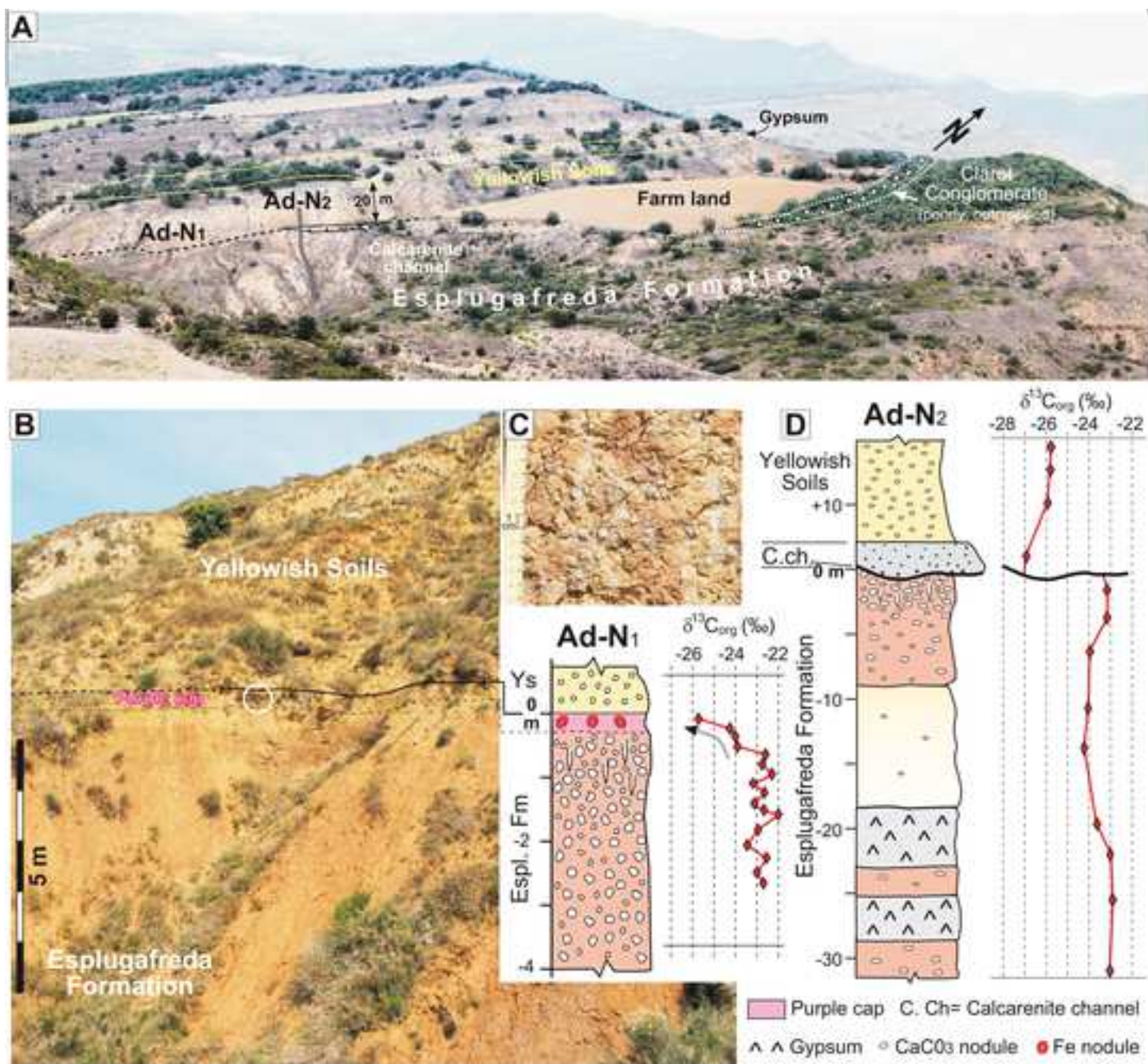
Pujalte et al Fig 8



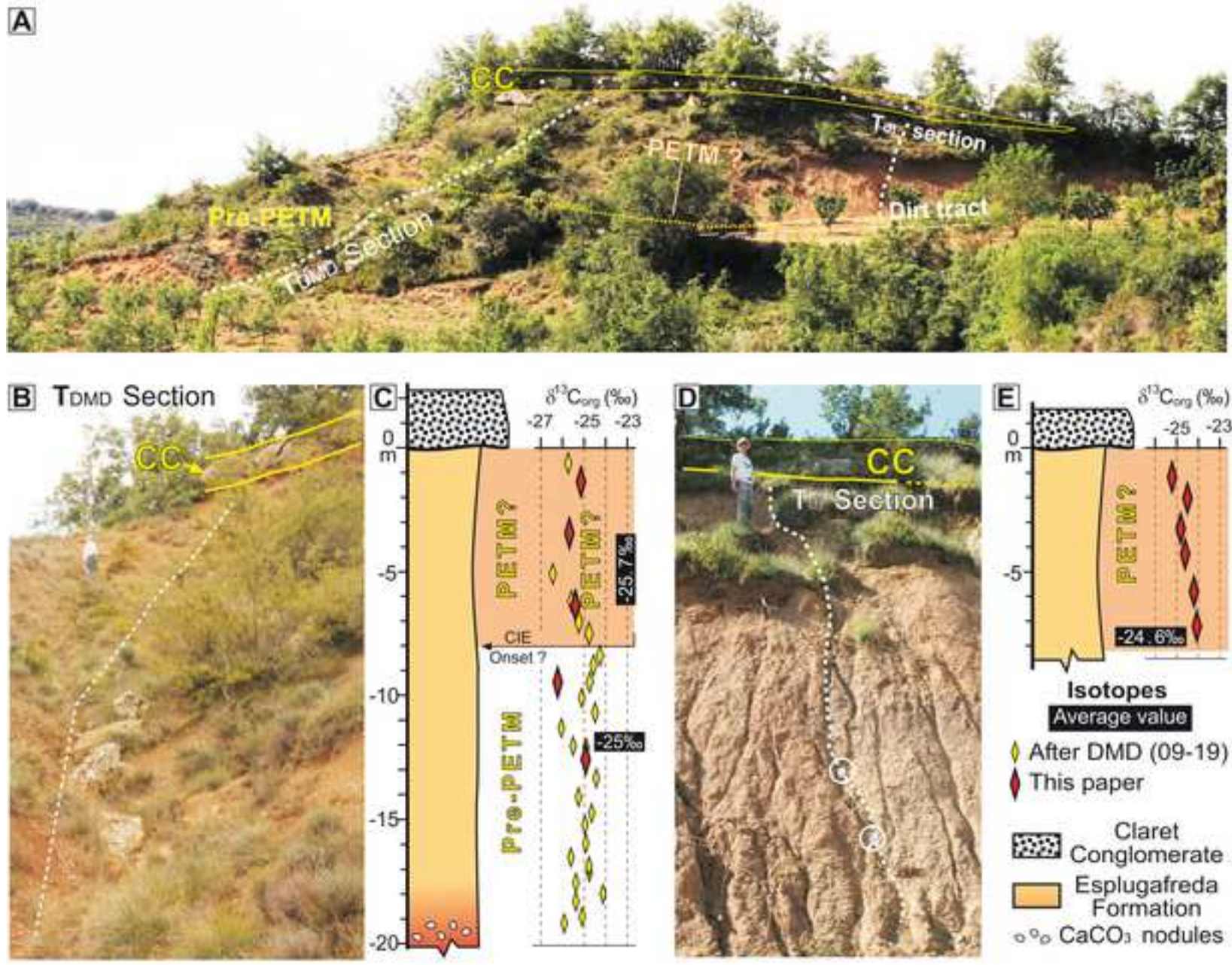
Pujalte et al Fig 9



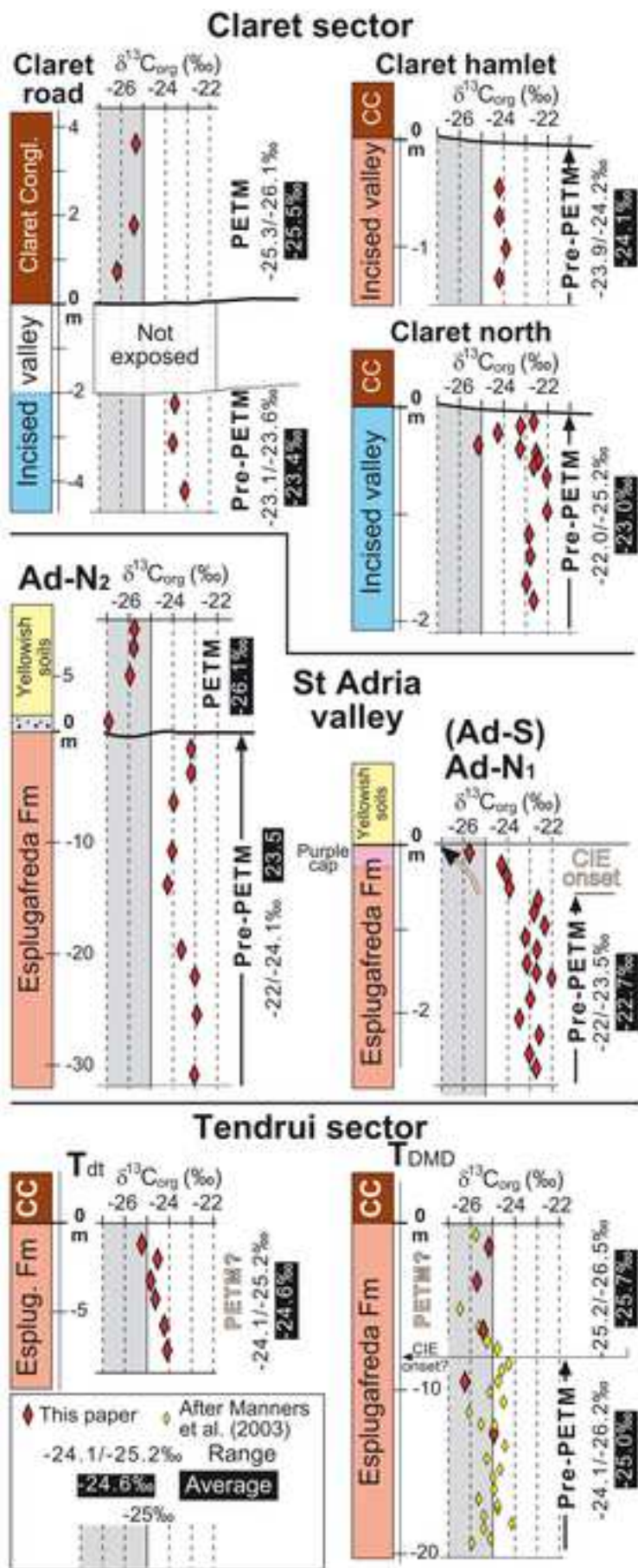
Pujalte et al Fig 10



Pujalte et al Fig 11



Pujalte et al - Fig 12



Pujalte et al Fig 13

Declaration of competing interest

The authors declare that they have no known competing financial interests or personal relationships that could have influenced the research reported in this paper